Electron Spin Resonance Experiments on Donors in Silicon. I. Electronic Structure of Donors by the Electron Nuclear Double Resonance Technique

G. Feher

Bell Telephone Laboratories, Murray Hill, New Jersey

(Received December 29, 1958)

The ground-state wave function of the antimony, phosphorus, and arsenic impurities in silicon has been investigated by means of the electron nuclear double resonance (ENDOR) method. By this method the hyperfine interactions of the donor electron with the Si^{29} nuclei situated at different lattice sites were obtained. The isotropic part of the hyperfine interaction agreed with the theory of Kohn and Luttinger to better than 50%. From a comparison of the experimental results with their theory a value for the conduction band minimum in silicon of $k_0/k_{max}=0.85$ ± 0.03 was obtained. So far no satisfactory theory exists to account quantitatively for the observed anisotropic part of the hyperfine interaction.

The observed line shape agreed with the shape predicted by summing up the individual hyperfine interactions which are the

cause of the broadening. The behavior of an inhomogeneously broadened line observed under adiabatic fast passage conditions is discussed in an appendix. The electronic g-values were measured with respect to the free carriers in a degenerate n-type silicon sample. The g-value of the free carriers was found to be 1.99875 ± 0.00010. The deviations of the donor g-values from the above value is several parts in 10^4 and increases monotonically with increasing ionization energy of the donors.

Besides the shallow donors Sb, P, and As, several other centers were investigated, but in considerably less detail. They include the chemical impurities Bi, Li, Fe, centers associated with the surface of the sample and with the heat treatment of silicon. The influence of substitutional germanium atoms on the resonance line in phosphorus-doped silicon has also been investigated.

I. INTRODUCTION

THE impurity center which results when a silicon atom is replaced by an element from the fifth column of the periodic table (e.g., phosphorus, arsenic, antimony) is called a donor. Four of the valence electrons of this impurity center form covalent bonds with their nearest silicon neighbors and therefore do not exhibit a paramagnetic resonance. It is the fifth electron that we will be concerned with in this paper. This electron moves in a Coulomb-like potential of the donor nucleus to which it is only loosely bound. At room temperature the donors are ionized and the electrons are free to move through the crystal. In this paper we will not discuss[1] the paramagnetic resonance of such a conduction electron[2,3] but will be concerned with its behavior when it is bound to the donor at low temperatures.

The first spin resonance absorption from bound donor electrons was reported by Fletcher *et al.*[4,5] They found a resonance pattern that consisted of $2I+1$ lines, where I is the nuclear spin of the donor atom. The spacing between the lines is proportional to the hyperfine interaction and provides information about $|\Psi(0)|^2$, the square of the electronic wave function at the donor nucleus. The magnitude of this quantity was satisfactorily explained by Kohn and Luttinger[6] who developed a detailed theory of the donor states. One of the main purposes of the present investigation was

to check the validity of this wave function by measuring the square of its value [i.e., the hyperfine (hf) interaction with the 5% abundant Si^2, nuclei] not only at the central donor nucleus but also at different silicon lattice points in the vicinity of the donor atom. Such a mapping out of the donor wave function is made possible by the electron nuclear double resonance[7] (ENDOR) technique which is described in some detail. The comparison of the theoretical and experimental hyperfine interactions hinges on the proper identification of the ENDOR lines. Because of the nature of the wave function the hf interactions with the Si^{29} nuclei do not fall off monotonically with their distance from the donor nucleus. This is due to interference effects between different parts of the wavefunction which depend critically on the position of the conduction band minimum in k-space. Although this makes the identification more difficult, once it has been accomplished, it provides a value for the position of the minimum. This information cannot be obtained from cyclotron resonance[8] experiments which tell us only the direction along which the minima lie.

The ENDOR technique is based essentially on the ability to change the spectral distribution of the electron spin resonance line by inducing low-frequency transitions. The applicability of this technique to different centers depends to a large extent on the magnitudes of the electron spin lattice relaxation and diffusion times. These are discussed in a separate paper[9] (to be referred to as Part II).

The measured electron spin resonance line width is caused by the hf interactions with the Si^{29} nuclei and is consistent with the experimentally determined values

[1] Except in comparing the g-value of the bound electron to the g-value of the free carriers (see Sec. II-E).

[2] Portis, Kip, Kittel, and Brattain, Phys. Rev. **90**, 988 (1953).

[3] F. K. Willenbrock and N. Bloembergen, Phys. Rev. **91**, 1281 (1953).

[4] Fletcher, Yager, Pearson, Holden, Read, and Merritt, Phys. Rev. **94**, 1392 (1954).

[5] Fletcher, Yager, Pearson, and Merritt, Phys. Rev. **95**, 844 (1954).

[6] W. Kohn and J. M. Luttinger, Phys. Rev. **97**, 1721 (1955); **98**, 915 (1955).

[7] G. Feher, Phys. Rev. **103**, 834 (1956).

[8] For a general discussion of cyclotron resonance see: Dresselhaus, Kip, and Kittel, Phys. Rev. **98**, 368 (1955).

[9] G. Feher and E. A. Gere, following paper [Phys. Rev. **114**, 1245 (1959)], this paper will be referred to as Part II.

of these interactions. In order to arrive at a meaningful line width a knowledge of the theory of the line shape as observed under adiabatic fast passage[10] conditions is necessary. This problem is discussed in an appendix.

The electron g values for the Sb, P, and As donors have been measured to a sufficiently high accuracy to detect the differences in the g shift between them. So far no theory is available for comparison.

Most of the work discussed in this paper is concerned with the three donors Sb, P, and As. In the course of the investigation resonances were also observed from other chemical centers (e.g., Bi, Li, Fe) and centers of less known structure (associated with the heat treatment of silicon and with the surface). They were investigated in considerably less detail and are discussed in Sec. III. The bismuth center is similar to the other group V donors but in view of its considerably higher ionization energy the effective mass theory of Kohn and Luttinger is less applicable to it. Lithium forms an interstitial center whose electron was found to have an anisotropic g value. Its wave function therefore cannot have tetrahedral symmetry. A discrepancy was found between the ratios of the hf interactions of Li[6] and Li[7] and the ratios of their respective nuclear g values. This "solid-state hyperfine anomaly" presumably arises from the different zero-point vibration amplitudes of the two isotopes. A single resonance line due to the iron impurity was observed. The electronic structure of this center is at present not understood. The parameters of the resonance line from the donors produced during the heat treatment of silicon varied from sample to sample. This is consistent with the present picture of a variety of centers being produced during the heat treatment. The "surface line" is apparently associated with the mechanical damage of the silicon surface, as determined from etching experiments. The influence of replacing a small percentage of silicon atoms by germanium was investigated in phosphorus-doped silicon. The main effect was a spread in the values of $|\Psi(0)|^2$ which resulted in a broadening of the resonance lines.

II. THE SUBSTITUTIONAL DONORS ANTIMONY, PHOSPHORUS, AND ARSENIC

(A) Energy Levels and Transitions

(1) The Spin Hamiltonian

We start by considering the magnetic interaction of a donor electron with the donor nucleus, the Si[29] nuclei that are encompassed in its orbit and the externally applied magnetic field H. The foregoing interactions are given by the spin Hamiltonian

$$\mathcal{3C} = -\mathbf{\mu}_e \cdot \mathbf{H} - \mathbf{\mu}_D \cdot \mathbf{H} - (8\pi/3)\mathbf{\mu}_e \cdot \mathbf{\mu}_D |\Psi(0)|^2$$
$$+ (8\pi/3)\sum_l \mathbf{\mu}_e \cdot \mathbf{\mu}_l |\Psi(\mathbf{r}_l)|^2 - \sum_l \mathbf{\mu}_l \cdot \mathbf{H}$$
$$+ \sum_l \frac{1}{(\mathbf{r}-\mathbf{r}_l)^3}\left\{ \mathbf{\mu}_l \cdot \mathbf{\mu}_e - \frac{3[\mathbf{\mu}_l \cdot (\mathbf{r}-\mathbf{r}_l)][\mathbf{\mu}_e \cdot (\mathbf{r}-\mathbf{r}_l)]}{(\mathbf{r}-\mathbf{r}_l)^2}\right\}, \quad (1)$$

[10] F. Bloch, Phys. Rev. **70**, 460 (1946).

where $\mathbf{\mu}_e$ is the electron magnetic moment, $\mathbf{\mu}_D$ the magnetic moment of the impurity nucleus, $\mathbf{\mu}_l$ the nuclear magnetic moment of a Si[29] at the lth lattice point, $\Psi(\mathbf{r}_l)$ the electronic wave function at the lth silicon site, $\mathbf{r}$ being measured from the position of the donor nucleus. The terms containing the square of the wave function represent the usual Fermi-Segrè hyperfine interactions. The last term in the Hamiltonian represents a dipole interaction and vanishes for an electronic wave function which has perfect cubic symmetry. Because of the symmetry of the wave function about the central donor atom the dipolar term as well as any quadrupole terms average to zero for this site. The Si[29] nuclei have a spin of one-half, and therefore cannot contribute to quadrupole effects but are responsible for the dipolar term in Eq. (1). From Eq. (1) we find for the energy of the system in the high-field approximation (i.e., $g\mu_0 H \ll$ remaining terms)

$$E = g\mu_0 H m_S + [a_D m_S m_D - (\mu_D/I_D)H m_D]$$
$$+ \sum_l [a_l m_S m_{\text{Si}} - (\mu_{\text{Si}}/I_{\text{Si}})H m_{\text{Si}}]$$
$$- \sum_l b_l m_S m_{\text{Si}}(1 - 3\cos^2\theta), \quad (2)$$

where m_S, m_D, m_{Si} are the magnetic quantum numbers for the electron, donor, and silicon nucleus, respectively, I is the spin of the nucleus under consideration, g = electron g-value, μ_0 = Bohr magneton, and

$$a_D = \frac{16\pi}{3}\frac{\mu_D}{I_D}\mu_e|\Psi(0)|^2,$$

$$a_l = \frac{16\pi}{3}\frac{\mu_{\text{Si}}}{I_{\text{Si}}}\mu_e|\Psi(\mathbf{r}_l)|^2, \quad (3)$$

$$b_l = \tfrac{1}{2}g\mu_0 \frac{\mu_{\text{Si}}}{I_{\text{Si}}}\left\langle \frac{3\cos^2\varphi - 1}{(\mathbf{r}-\mathbf{r}_l)^3}\right\rangle.$$

The last term in Eq. (2) was obtained by assuming that $b_l \ll a_l$ and that the wave function has axial symmetry about $\mathbf{r}_l$. θ is the angle between this axis of symmetry and the external magnetic field, and φ is the angle between $(\mathbf{r}-\mathbf{r}_l)$ and the axis of symmetry. The two previous assumptions are not justified for some of the observed lines and will be removed when we come to analyze the transitions in question (see Sec. C-2). In an ordinary microwave resonance experiment one induces the transitions $\Delta m_S = \pm 1$; $\Delta m_D = 0$; $\Delta m_{\text{Si}} = 0$. This results in a set of hyperfine lines which in our case are resolved and occur at

$$h\nu_e = g\mu_0 H + a_D m_D, \quad (4)$$

where m_D ranges from I, $I-1 \cdots -I$ and ν_e is the microwave frequency.[11] The terms involving $m_S m_{\text{Si}}$ do not give rise to resolved hyperfine lines but only contribute to the broadening of the observed microwave

[11] In practice one varies the magnetic field rather than the microwave frequency which in the high field approximation is equivalent.

transitions. This point is more fully discussed in the next section.

In the ENDOR technique transitions for which $\Delta m_S = 0$ are observed, and one flips either the donor nucleus ($\Delta m_D = \pm 1$) or the Si^{29} nuclei ($\Delta m_{Si} = \pm 1$).

For the transitions of the donor nucleus we get a set of lines at a frequency ν_D given by

$$h\nu_D{}^{\pm} = |\tfrac{1}{2}a_D \mp (\mu_D/I_D)H|, \qquad (5)$$

where the upper sign refers to the $m_S = +\tfrac{1}{2}$ and the lower to the $m_S = -\tfrac{1}{2}$ set of levels (see Fig. 1). Since for such transition $\Delta m_S = 0$ and $\Delta m_{Si} = 0$, the $\Delta m_{Si}\Delta m_S$ terms do not contribute to the line width [see Eq. (2)]. This is the reason why the ENDOR line width can be many orders of magnitudes smaller than the microwave electron spin resonance line width and therefore results in greatly improved resolution. This is only true as long as the electronic wave function of each center is the same. Differences in the wave function will broaden the ENDOR lines with a corresponding loss in resolution. This situation has been encountered for example in phosphorus-doped silicon when a small percentage of Ge was added to the crystal. (See Sec. III F.) Another source of broadening in imperfect single crystals may arise from the anisotropic part of the wave function. If the center exhibits an isotropic line, a single crystal is not required. We have powdered a silicon crystal (400 mesh) and found no broadening of the phosphorus (a_D) ENDOR lines.

The transition frequency for flipping the lth Si^{29} nucleus obtained from Eq. (2) is given by[12]

$$h\nu_l{}^{\pm} = |-(\mu_{Si}/I_{Si})H \pm \tfrac{1}{2}a_l \mp \tfrac{1}{2}b_l(1 - 3\cos^2\theta)|. \qquad (6)$$

Equation (6) represents two sets of lines centered around the unperturbed Larmor frequency of a Si^{29} nucleus in an external field H (~ 2.6 Mc/sec at 3000 oersteds). In all of our work only the higher frequency set of lines was analyzed.

(2) The Energy Level Diagram

The energy level diagram of the system discussed in the previous section is shown in Fig. 1 in which we consider for simplicity a donor having a spin of one-half (e.g., phosphorus). The main splitting $h\nu_e$ [see Eq. (4)] is due to the electron spin in the external magnetic field and occurs at a microwave frequency. The next smaller splitting $h\nu_D{}^{\pm}$ [see Eq. (5)] due to the hyperfine interaction with the donor is of the order of tens of Mc/sec and in our case can still be resolved by ordinary paramagnetic resonance methods (see Fig. 2). The hyperfine splitting $h\nu_l{}^{\pm} - H\mu_{Si}/I_{Si}$ [Eq. (6)] due to the Si^{29} nuclei ranges from a few Mc/sec to essentially zero for those Si^{29} nuclei that are far removed from the donor and therefore do not interact with the electron

[12] Note that when $|\tfrac{1}{2}a_l - \tfrac{1}{2}b_l(1 - 3\cos^2\theta)| \gg (\mu_{Si}/I_{Si})H$, the upper levels in the Breit-Rabi diagram have crossed and Eq. (6) becomes $h\nu_l{}^{\pm} = |\tfrac{1}{2}a_l - \tfrac{1}{2}b_l(1 - 3\cos^2\theta) \mp (\mu_{Si}/I_{Si})H|$.
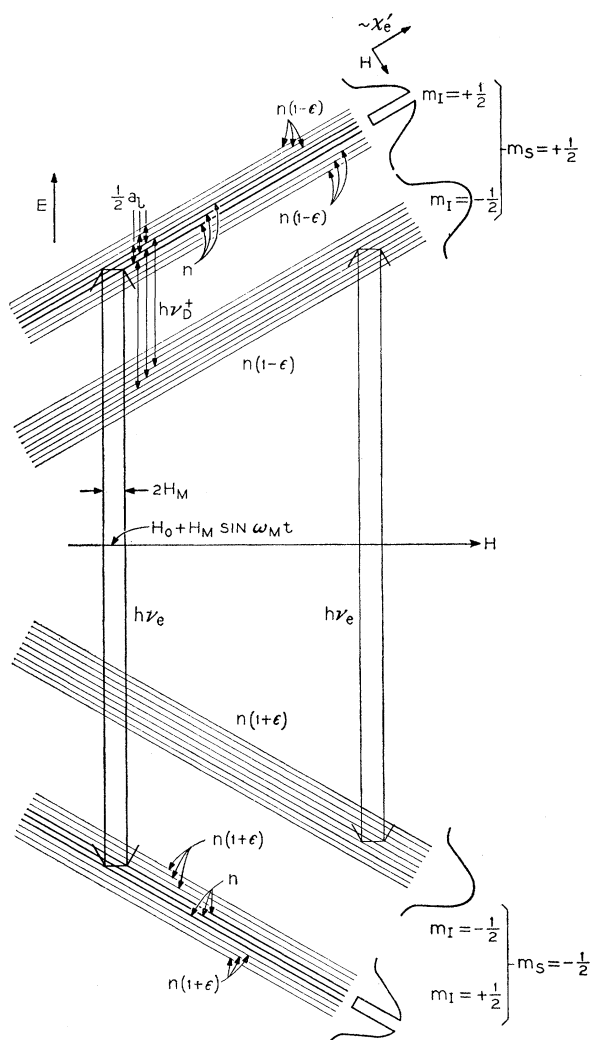

FIG. 1. Schematic representation of the energy level diagram of a donor electron in phosphorus-doped silicon. We assume for simplicity that the microwave field completely saturates part of the $m_I = +\tfrac{1}{2}$ line. In the ENDOR technique a partial desaturation (i.e., increase in signal) is observed when the a_l or a_D transitions are induced.

spin. In Fig. 1 these interactions are drawn for the sake of simplicity as discrete levels although the width of each level is actually larger than the spacing between them. In an ordinary electron spin resonance experiment these levels are therefore not resolved but are the cause of the observed line width. By means of the ENDOR technique, one can resolve and accurately measure these small interactions.

(B) The ENDOR Technique

(1) Discussion of the Technique

The ENDOR technique is based on the fact that a small part of an inhomogeneously broadened resonance line may be saturated without appreciably affecting the rest of the line. This is made possible because different

parts of the line arise from different donors whose resonant frequencies have been modified by the effective magnetic fields created by the hyperfine interactions from various Si^{29} configurations within the donor orbit. This behavior is just the defining property of an inhomogeneously broadened line as discussed by Portis[13] in connection with F centers.

In the ENDOR experiments one sets the magnetic field H_0 to the center of the microwave resonance line and applies an additional variable radio-frequency field at right angles to it. The electron resonance absorption is now saturated by applying a sufficiently strong microwave field, thereby decreasing the observed electron resonance signal. This situation is indicated in Fig. 1. The population of the upper and lower electronic states is equal corresponding to complete saturation and hence the signal is zero. Here n is the total number of donors (i.e., unpaired spins) divided by the number of levels indicated. The remaining levels are undisturbed and their occupancy is given by the electronic Boltzmann factor $\epsilon = \mu_0 H/2kT$ as indicated. If one now sweeps the radio-frequency field covering the frequency $h\nu_D^{\pm}$ or $h\nu_l^{\pm}$ the population of the previously saturated levels will change. This change may be accomplished either by going through the nuclear transitions under adiabatic fast passage conditions[10] thereby reversing the population, or by saturating the nuclear transitions thereby equalizing the populations. In the first mode of operation the population of the electronic level should change by ϵ, in the second by $\epsilon/2$. This change in population manifests itself as a change in the *electron* resonance signal and is recorded together with the nuclear frequency at which this change occurs.

The foregoing discussion is illustrated for phosphorus-doped silicon in Fig. 2. The saturated middle region of the $m_I = +\frac{1}{2}$ line demonstrates the inhomogeneous nature of the line. The trace was obtained by setting the magnetic field H_0 on the center of the $m_I = +\frac{1}{2}$ line and modulating it by an amount $H_M \cos\omega_M t$; the modulation frequency in our experiments was 100 cps. The microwave magnetic field was then turned on and the central portion of the line was saturated. The
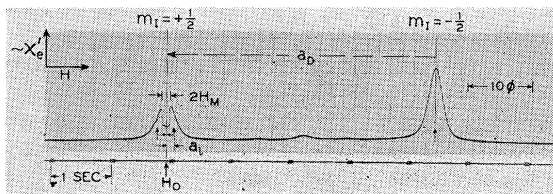

FIG. 2. Demonstration of the inhomogeneous broadening of the donor resonance in phosphorus-doped silicon (5×10^{16} P/cm³, $T=1.25°$K, $H\approx3000\phi$). The center of the $m_I = +\frac{1}{2}$ line was saturated prior to the traversal. In the ENDOR technique the field is set to H_0. An additional rf field flips the spin packets as indicated by the arrows thereby desaturating the electron spin resonance line.

[13] A. M. Portis, Phys. Rev. 91, 1071 (1953).

dynamics of this saturation process is described in Appendix A-3. Upon sweeping subsequently through the two lines, the trace of Fig. 2 was obtained. One sees clearly that one can "burn a hole"[14] of width $2H_M$ in the center of the resonance line without affecting the rest of it. It is of course important that the time interval between the saturation process and the sweep through the line be small in comparison with the spin-lattice relaxation and diffusion time (see Part II). The small line in the central region of the pattern in Fig. 2 is due to exchange interactions with neighboring donors.[15] We will not be concerned with such effects in the present investigation.

In the ENDOR experiments the field remains set to $H_0 + H_M \cos\omega_M t$. The spin packets indicated by broken arrows in Fig. 2 may then be transferred into the "hole" by applying a field of the appropriate transition frequency. The "filling up" of the hole causes the observed increase in the electron spin resonance signal. In order to demonstrate this effect more clearly the value of $2H_M$ used to obtain Fig. 2 was chosen to be 1.5 oersteds. In the actual experiments a ten times smaller field modulation was used.

(2) Experimental Results

The result of the double resonance experiment on P-doped silicon with an impurity concentration[16] of 5×10^{16} P/cm³ is shown in Fig. 3. In the present work we are mainly concerned with the small part of the spectrum that corresponds to the hyperfine interaction with the Si^{29} nuclei. However, before discussing it in greater detail let us consider briefly the behavior of the electron resonance signal as one sweeps the entire available radio-frequency range.

The upper trace [Fig. 3(a)] shows the increase in signal when the two donor hf interaction frequencies are traversed. The steep rise of the line is due to the small inherent line width of the spin packets, whereas the slow trailing off is associated with the time required to resaturate the line as discussed in Appendix A-3. We notice also that the second line that is traversed is larger than the first. This is the consequence of the redistribution of the population after the first traversal and has been discussed in detail elsewhere.[17]

The second trace [Fig. 3(b)] is the one of main interest. It arises from the hf interactions with the Si^{29} nuclei. We notice that some lines exhibit additional splittings which arise from the anisotropic part of the

[14] Such "hole burning" experiments were first reported on nuclear system by Bloembergen, Purcell, and Pound, Phys. Rev. 73, 679 (1948).

[15] C. P. Slichter, Phys. Rev. 99, 479 (1955); Feher, Fletcher, and Fere, Phys. Rev. 100, 1784 (1955).

[16] The impurity concentration in this part of the work was obtained from room-temperature resistivity measurements. For the latest values for the mobilities see for instance E. M. Conwell, Proc. IRE 46, 947 (1958). In Part II an exact knowledge of the impurity concentration is of greater importance and was obtained from Hall effect measurements.

[17] J. Eisinger and G. Feher, Phys. Rev. 109, 1172 (1958).

hyperfine interaction [see Eq. (2)]. The magnitude of these splittings is the largest for the most tightly bound donor, i.e., the one having the largest ionization energy. This turns out to be the As donor which was therefore investigated in more detail than the other two. The traces of the spectrum of interest for As-doped silicon are shown in Fig. 4 with the magnetic field pointing along a different principal crystalline direction in each of the traces. In order to obtain a more detailed picture of the anisotropic variations, the angle between the magnetic field and the crystalline axis was varied in steps of 5°. The nuclear frequency in those measure-
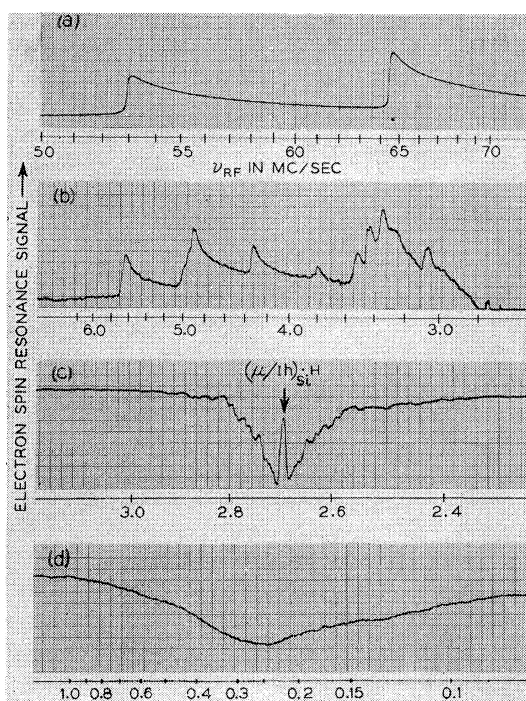
FIG. 4. The ENDOR signal from arsenic-doped silicon (8×10^{16} As/cm^3, $T = 1.25°$K, $\nu_e \approx 9000$ Mc/sec). The lines represent the hf interaction of the donor electron with the Si^{29} nuclei at different lattice points. Note the change in the structure of the lines when the magnetic field points along the different crystalline directions. For the analysis of this anisotropic interaction the rate of frequency sweep was reduced (see Fig. 13).

FIG. 3. Variation of the microwave electron spin resonance signal with the application of an additional rf field. The sample is phosphorus-doped silicon (5×10^{16} P/cm^3, $T = 1.25°$K, $H_0 \approx 3000$ oersteds). Figure 3(a) shows the increase in signal when the donor hf interaction frequencies are traversed. Figure 3(b) arises from the hf interaction with Si^{29}'s located at different lattice points (see also Figs. 4 and 13). Figure 3(c) is due to the hf interactions with Si^{29}'s which are far removed from the donor. The decrease in signal in Fig. 3(d) is due an effect akin to rotary saturation.[19]

ments was swept at a much slower rate than shown in Fig. 4 in order to improve the accuracy with which the splittings could be determined. (See Sec. II C-2 and in particular Fig. 13.) The ENDOR line width is approximately 10 kc/sec which is to be compared with ~10 Mc/sec for the electron resonance line width. Thus the double resonance technique improved the resolution by three orders of magnitude. The anisotropic part plays an important role in the identification of the lines and is discussed more fully in Sec. II C-2. For the Sb and P donors the experiments were performed with
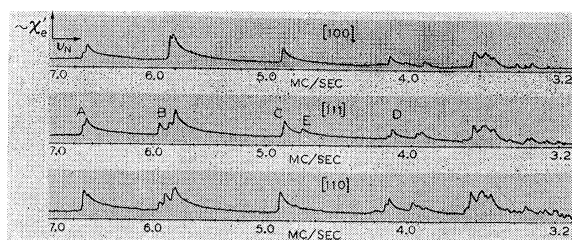
the magnetic field pointing only along the three principal crystalline axes.

The trace of Fig. 3(c) arises from Si^{29} nuclei which are far removed from the donor. Their hf interaction is very small and cannot be resolved. Since there is a large number of such distant silicons the integrated signal is considerably larger than that due to the nearby silicons. There are several interesting features associated with this trace. First we see that the electronic signal decreases when the hf transitions are being induced. This would be impossible under the conditions depicted in Fig. 1, in which complete saturation (i.e., no signal) was assumed. In practice one does not, however, saturate the line completely (as indeed is indicated in Fig. 2) and therefore a reduction in signal is not excluded. This reduction in signal starts approximately at a splitting given by the radio-frequency $\nu_N \sim g\mu_0 H_M/h$. This suggests that when spin packets are flipped *within* the width of the saturated part of the resonance line a reduction in signal occurs. This presumably is the result of a de-phasing process between spin packets. The notch that occurs at the rf frequency $\nu_N = (\mu_{Si}/I_{Si}h)H$ may be explained as follows: the Si^{29} nuclei whose resonant frequencies are unperturbed and therefore occur at the above ν_N do not interact with the electron (otherwise their resonant frequency would be shifted). Since they do not interact there is no reason why the electronic signal should be affected by them. The signal therefore tries to return to its undisturbed saturated value $\chi_{e \text{ SAT}}'$. The pattern should be symmetrical about the frequency $\nu_N = (\mu_{Si}/I_{Si}h)H$ [see Eq. (6)]. The observed small asymmetry is presumably due to relaxation effects.

In a phosphorus-doped silicon sample which was 10% compensated with boron an additional line was observed at the unperturbed Larmor frequency of the P^{31} nucleus. This signal arises from the phosphorus sites that have lost their donor electrons to the boron acceptors. The nuclei at those sites are only weakly coupled to the neighboring donors and therefore resonate at approximately the unperturbed frequency. This effect may be of importance if one wants to study

the nuclear resonance of centers that are not paramagnetic or whose resonance signal does not satisfy the conditions necessary to observe an ENDOR signal directly. If such centers are placed in the vicinity of "proper" paramagnetic centers the effect of flipping their nuclei may be investigated via the electron spin resonance signal of the nearby paramagnetic centers.

Figure 3(d) shows a gentle reduction of the signal which has nothing to do with the Si[29]'s.[18] The position of the dip is affected by the strength of the microwave magnetic field H_1. This suggests that this phenomenon might be akin to the *rotary saturation* effect discussed by Redfield[19] for the case of a saturated nuclear system.

(3) The Experimental Equipment

The spectrometer used in this work operates at X-band ($\nu_e \simeq 9000$ Mc/sec). It is a balanced bridge type so that the observed signal can be made proportional either to the real or imaginary part of the susceptibility. All the ENDOR experiments were done at 1.25°K. At this temperature the relaxation times are long and therefore the bridge was always tuned to the dispersion mode and the signals were observed under adiabatic fast passage conditions (see Appendix A). The spectrometer employs a superheterodyne detection scheme with an intermediate frequency of approximately 60 Mc/sec. The ordinary electron spin resonance signals may be obtained in two different ways. One way is to connect the output of the i.f. detector to the recorder and sweep through the electron resonance
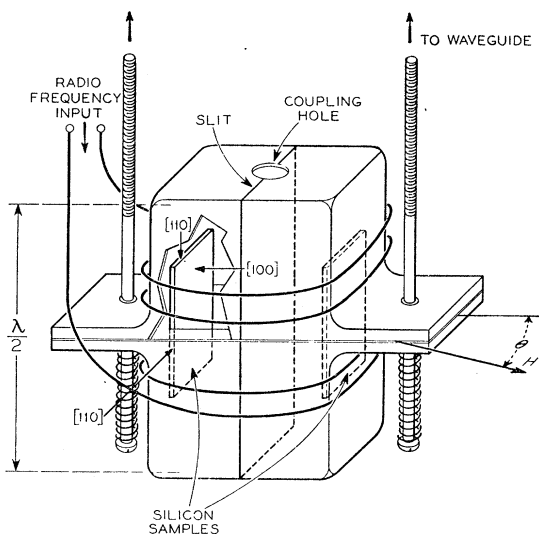

FIG. 5. Microwave cavity assembly with silicon samples and rf coil. The cavity is molded out of Pyrex and coated on the inside with silver. The slit in the coating reduces rf eddy currents. The magnetic field may be rotated in the (110) plane of the samples as indicated.

lines without magnetic field modulation. This method is not very sensitive but is more straightforward and eliminates complications which may arise when field modulation schemes are used. In the ENDOR experiments where a higher sensitivity is required the magnetic field is modulated at 100 cps. A signal of this frequency is thus observed when passing through a resonance line and is detected by a phase-sensitive detector which follows a 100-cps audio amplifier. Its output has an integrating network and is fed into the recorder.

The rectangular microwave cavity operates in the TE_{101} mode and is illustrated in Fig. 5. It is molded out of Pyrex and coated on the inside with silver paint.[20] It consists of two $\lambda/4$ sections in order to avoid breaks in the microwave currents. Slits were provided in the silver paint to allow the nuclear frequency, necessary for the ENDOR experiments, to penetrate into the cavity. The unloaded Q of such a cavity at liquid helium temperatures is about 5000. The silicon samples were cut along the principal crystalline directions as indicated in Fig. 5 and held in place with styrofoam which filled the entire cavity. This cuts down the amount of helium that enters the cavity and thereby reduces the noise which arises from helium bubbles above the λ point. The sample dimensions were 9 mm $\times$ 15 mm $\times$ 1 mm and for most of the ENDOR experiments contained between $4-8 \times 10^{16}$ donors/cm^3. The rf is applied to a coil wrapped on the outside of the cavity. The coil is untuned and terminates a 50-ohm coaxial line. The rf power is obtained from a commercial bench oscillator[21] with a modified motor driven frequency dial. In order to improve the match into the coil the output of the oscillator was fed into a cathode follower. A more detailed discussion of the rest of the spectrometer is given elsewhere.[22]

(C) Comparison of Experimental Results with Theory

(1) The Theoretical Wave Function

We will start by reviewing, briefly, the results of the theory of shallow donor states in silicon developed by Kohn and Luttinger.[6] They show that the wave function of a donor electron in its ground state can be approximately represented by a linear combination of six wave functions corresponding to the six minima of the conduction band which for silicon lie along the [100] direction. The wave functions have the form:

$$\Psi(\mathbf{r}) = \left(\tfrac{1}{6}\right)^{\frac{1}{2}} \sum_{j=1}^{6} F^{(j)}(\mathbf{r}) u^{(j)}(\mathbf{r}) \exp(i\mathbf{k}_0{}^j \cdot \mathbf{r}), \qquad (7)$$

where j refers to the different minima, $u^{(j)}(\mathbf{r}) \exp[i\mathbf{k}_0{}^j \cdot \mathbf{r}]$ is the Bloch wave at the jth minimum and $F^{(j)}(\mathbf{r})$ is a

[18] A similar behavior was found in an experiment performed on triphenylmethyl [Weissmann, Feher, and Gere, J. Am. Chem. Soc. **79**, 5584 (1957)].

[19] A. G. Redfield, Phys. Rev. **98**, 1787 (1955).

[20] The silver paint used was Du Pont No. 4545. It is fired at 550° and adheres very well to Pyrex.

[21] Hewlett-Packard oscillators No. 650A and No. 608C.
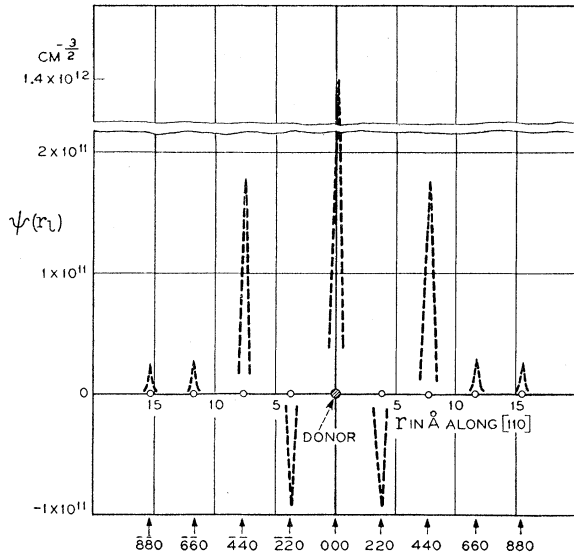
[22] G. Feher, Bell System Tech. J. **26**, 449 (1957).

FIG. 6. Wave function of donor electron in arsenic-doped silicon along the [110] direction, after theory of Kohn and Luttinger, assuming $k_0/k_{max}=0.85$. Note that the wave function does not fall off monotomically with the distance from the donor. The largest hf interaction in this direction occurs with the Si[29]'s at the 440 site.

hydrogen-like envelope function obtained by solving an effective mass Schrödinger equation into which the observed binding energy of the donor has been substituted.

From Eq. (7) we see that at the donor site ($r=0$) the six wave functions add and $|\Psi(0)|^2$ has an appreciable value. However, as r increases, the $\exp(i\mathbf{k}_0{}^j\cdot\mathbf{r})$ terms will cause the six wave functions to interfere with each other. One would expect therefore the hyperfine interaction with the donor nucleus ($r=0$) to be stronger than with the Si[29] nuclei, which indeed is found to be the case. Since the interference effects depend on the position of the conduction band minima a comparison of the experimental ENDOR results with theory should give a value for k_0. The difficulty of this comparison lies in the fact that due to the interference effects the wave function at the lth silicon, $|\Psi(\mathbf{r}_l)|^2$, does not decrease monotonically with increasing $\mathbf{r}_l$. One is faced therefore with the problem of correlating the observed experimental frequency of each line with the hyperfine interaction of a silicon at a specific lattice site $\mathbf{r}_l$. This point is illustrated schematically in Fig. 6 in which the wave function for the arsenic donor is sketched along the [110] direction. In this plot, $|\Psi(0)|^2$ is taken from experiment and the $|\Psi(\mathbf{r}_l)|^2$ are computed from Eq. (9). For the k_0 chosen ($k_0/k_{max}=0.85$ which is the actual value obtained in Sec. II C-3), one sees that the hyperfine interaction with the 440 silicon is much stronger than with the 220 silicon in spite of the latter being closer to the donor. The labeling of the lattice sites is such that four units correspond to the edge of the unit cell, which is 5.43×10^{-8} cm (see also Fig. 7).

Another important parameter that enters into the theory is the amount by which the conduction band wave function $u^{(j)}(\mathbf{r})$ is concentrated at the lattice site $\mathbf{r}_l$. This is conveniently expressed by the dimensionless quantity η defined as

$$\eta = |u^{(j)}(\mathbf{r}_l)|^2 / \langle u^{(j)}(\mathbf{r})\rangle^2_{Av}, \qquad (8)$$

where the average is taken over the unit cell.

The quantity η has been estimated from nuclear relaxation time measurements by Shulman and Wyluda.[23] They obtained the value 186 ± 18 which was used in this paper.

The experimental results discussed in the next section show that the main hyperfine interaction is isotropic and arises from the contact term which is proportional to $|\Psi(\mathbf{r}_l)|^2$. By expanding Eq. (7), one obtains

$$|\Psi(\mathbf{r}_l)|^2 = \tfrac{2}{3}\eta[F^{(x)}(\mathbf{r}_l)\,\cos k_0 x_l + F^{(y)}(\mathbf{r}_l)\,\cos k_0 y_l \\ + F^{(z)}(\mathbf{r}_l)\,\cos k_0 z_l]^2, \qquad (9)$$

where x_l, y_l, z_l are the coordinates of the lth silicon measured from the donor along the [100] directions (see Fig. 8). The normalized anisotropic envelope function $F_l^{(x)}(\mathbf{r}_l)$ may be approximated by[24,25]

$$F^{(x)}(\mathbf{r}_l) = F(\mathbf{r}_l)_{isotr}\left\{\left(\frac{a^{*3}}{a^2b}\right)^{\tfrac{1}{2}}\exp\left[-\left(\frac{y_l^2+z_l^2}{(na)^2}\right.\right.\right. \\ \left.\left.\left. +\frac{x_l^2}{(nb)^2}\right)^{\tfrac{1}{2}}\right]\Big/\exp\left[-\left(\frac{r_l}{na^*}\right)\right]\right\}, \qquad (10)$$
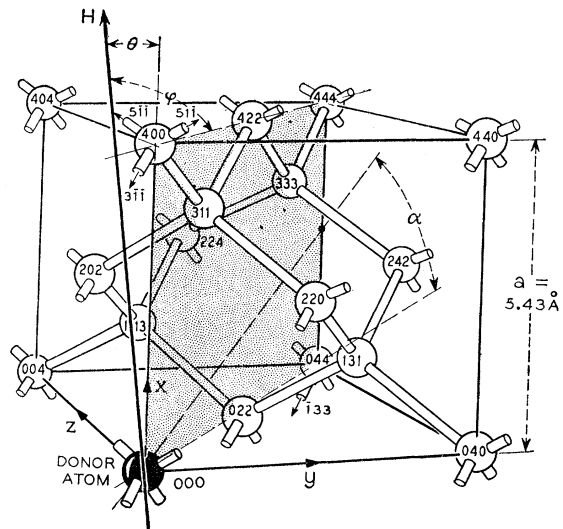

FIG. 7. Silicon crystal with a substitutional donor. In order to obtain the symmetry of the anisotropic hf interaction the magnetic field is rotated in the (110) plane (see shaded area). From an inspection of the lattice it can be seen that the 400 site does not have axial symmetry. The principal axis of the anisotropic hf interaction corresponding to the 440 site makes an angle α with the [110] direction.

[23] R. G. Shulman and B. J. Wyluda, Phys. Rev. 103, 1127 (1956).
[24] W. Kohn, in Solid-State Physics, edited by F. Seitz and D. Turnbull (Academic Press, Inc., New York, 1957), Vol. 5.
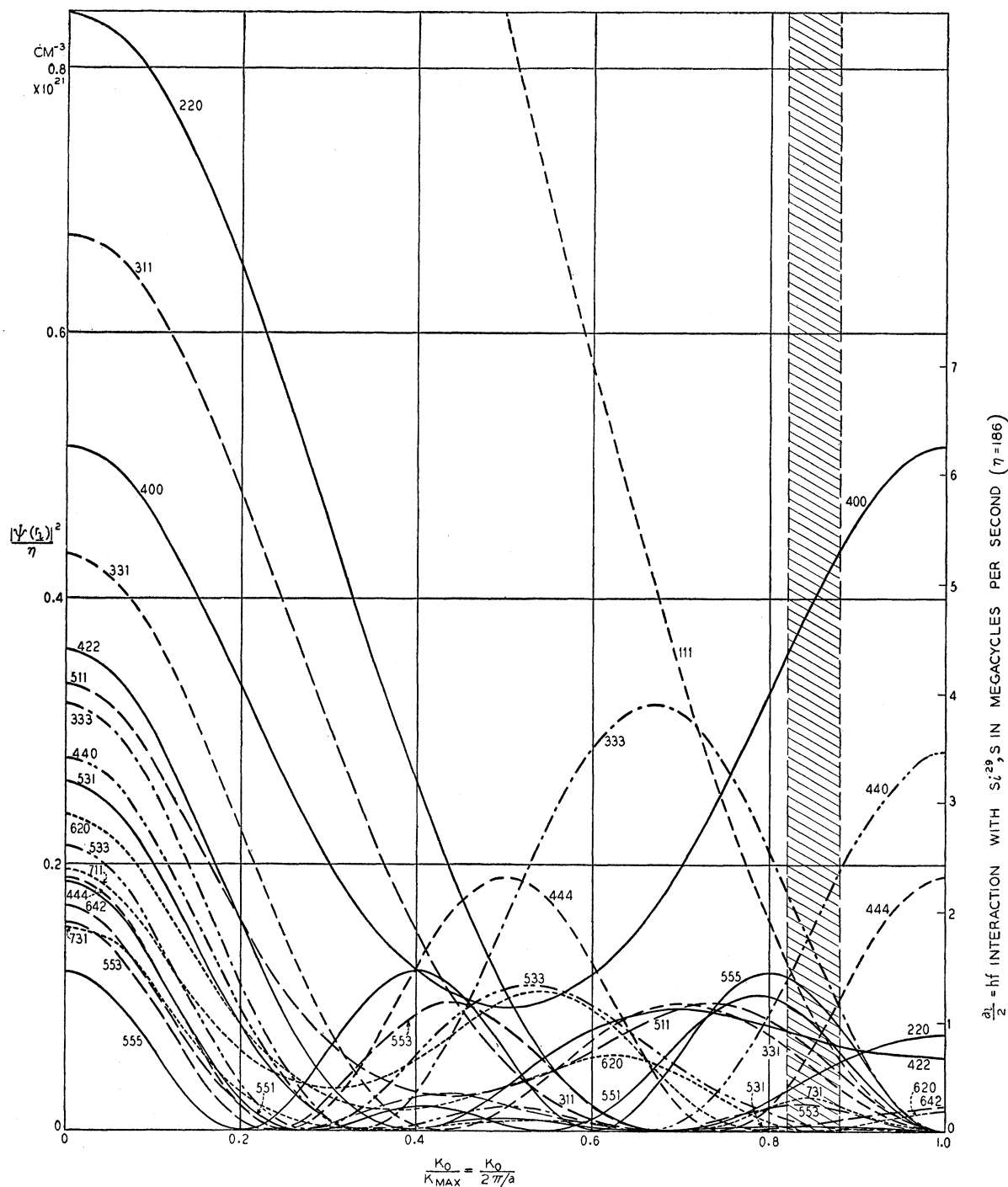[25] W. Kohn (private communication).

FIG. 8. The square of the electron wave function $|\Psi(r_i)|^2$ in arsenic-doped silicon as a function of the position of the conduction band minimum $k_0/k_{\max}$ for different silicon lattice sites (see Fig. 8). The graph was calculated by Schechter and Mozer from the theory of Kohn and Luttinger[6] [see Eq. (9)]. The shaded area indicates the position of $k_0/k_{\max}$ obtained from a comparison of the experimental data with theory.

where $F(\mathbf{r}_i)_{\mathrm{isotr}}$ is the envelope function obtained by solving an isotropic effective mass equation using the observed ionization energy and the expression in brackets is an anisotropy correction. For silicon the parameters entering Eq. (10) are: $a=25.0\times10^{-8}$ cm,

$b=14.2\times10^{-8}$ cm, $a^*=21.0\times10^{-8}$ cm, and $n=(0.029/E_i)^{\frac{1}{2}}$, E_i being the observed donor ionization energy in electron volts. The x-axis above is defined by the direction of the k vector.

Similar expressions are obtained for $F^{(y)}$ and $F^{(z)}$ by

appropriate permutations of x_l, y_l, z_l. The anisotropy of the envelope function as seen from Eq. (10) arises from the difference between the longitudinal and transverse effective masses ($m_l = 0.98 m_0$, $m_t = 0.19 m_0$) which causes the wave function to be compressed along the [100] direction. Schechter and Mozer[26] have calculated Eq. (9) for different values of k_0. Their results are plotted in Fig. 8 for a donor having an ionization energy of 0.050 ev corresponding approximately to the As donor.[27] Similar plots were obtained for $E_i = 0.040$ ev and 0.045 ev corresponding to the Sb and P donors.[27]

(2) Identification of the Lines

As was pointed out earlier the interference effects make the identification of the lines a difficult task. If one had only the experimental values of the isotropic part of the hyperfine interaction, such an identification would be nearly impossible. Fortunately, there are two additional pieces of information available which help in the identification. One is the relative amplitudes of the ENDOR lines which have to be consistent with the number of equivalent occupied lattice points and the other is the additional structure on each line. From the angular variation of this structure one can find the symmetry of the particular lattice point with respect to the impurity center. After one or two lines have been identified one can use the theoretical curves of Fig. 8 to obtain a rough value of k_0/k_{max} and thereafter use Fig. 8 as a convenient guide to check the assignment of the remaining lines.

To illustrate the method we shall now analyze several lines of the ENDOR spectrum for As-doped silicon. The lines of the spectrum are labeled in Fig. 4.

(a) Line A.—This line is due to the Si^{29} nuclei which exhibit the largest hf interaction (see Fig. 4). It will be shown presently that this interaction arises from the silicons situated at the 400 site (fourth nearest neighbor). An inspection of Fig. 7 reveals that this site does not have axial symmetry. This is readily seen by looking along the [400] direction and noting that the two 311 sites are nearer to the donor than the two 511 sites, thereby destroying the axial symmetry. One would expect therefore that the principal axes of the 400 site lie: one in the [100] direction and the other two in the two nonequivalent [110] directions. In Sec. II A-1 we derived the angular dependence for the anisotropic hf interaction assuming axial symmetry. For the case of nonaxial symmetry Eq. (6) should be modified to have the form[28]

$$h\nu_l^{\pm} = |-(\mu_{Si}/I_{Si})H \pm \tfrac{1}{2}a_l \mp \tfrac{1}{2}b_l(1-3\cos^2\theta)$$
$$\mp \tfrac{1}{2}b_l'(1-3\cos^2\varphi)|, \quad (11)$$

[26] D. Schechter and B. Mozer (private communication).

[27] Morin, Maita, Shulman, and Hanney, Phys. Rev. 96, 833. The value of 0.039 ev given for P is a misprint and should read 0.044 ev. The fact that we used 0.001 ev higher values in our plots has a negligible effect on the results.

[28] That this is the right form can be easily seen by decomposing the nonaxial case into two axial ones at right angles to each other.
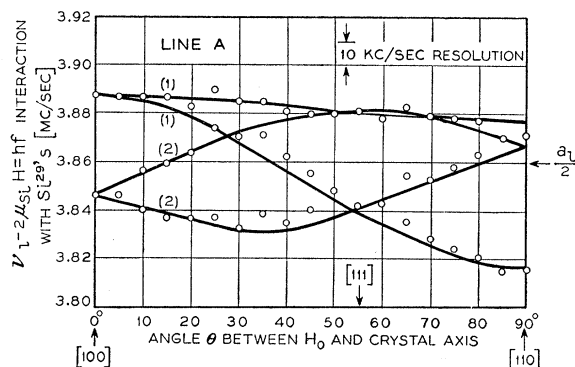
FIG. 9. Hf interaction of the donor electron in As-doped silicon with the Si^{29} nuclei at the 400 site (see Fig. 8). The magnetic field is rotated in the (110) plane of the crystal, angles are measured from the [100] direction. The full lines represent the theoretical fit given by Eq. (11). This site does not have axial symmetry.

where θ is the angle that the magnetic field makes with one principal axis (in this case the [100] direction) and φ is the angle it makes with the other principal axis (in this case one of the [110] axes,[29] see Fig. 7). The quantities a_l, b_l and b_l' are the amplitudes of the hf interactions and may be obtained by fitting Eq. (11) to the experimentally determined hf interactions.

Figure 9 shows a plot of the hf interaction for the As donor as a function of the angle between H and the crystalline axis. The magnetic field is rotated in the (110) plane of the crystal (see shaded area in Fig. 7) so that it can lie along all the three principal crystalline directions. The circles are the experimentally determined points and the theoretical fit with $\tfrac{1}{2}a_l = 3.86$ Mc/sec, $\tfrac{1}{2}b_l = 0.023$ Mc/sec, $\tfrac{1}{2}b_l' = 0.020$ Mc/sec is indicated by full lines. The numbers in parentheses indicate the expected relative amplitudes of the lines. They are obtained by considering which of the six 400 sites are equivalent when the magnetic field is applied and are in agreement with the experimentally observed amplitudes. The good fit of the experimental points with the predicted curves gives us confidence that the assignment of this line is correct. The only other sites with the same symmetry properties are the sites 800, 1200, etc. However, they can be safely excluded on account of their much lower hf interactions.

By comparing $\tfrac{1}{2}a_l$ of this line with the predicted hf interactions of Fig. 8 we find that k_0/k_{max} must be in the vicinity of ~ 0.8 or 0.2. The 0.2 value can be excluded because the observed 400 line exhibits the largest hf interaction in accord with the ~ 0.8 value. A more accurate value of k_0/k_{max} will be obtained after all the lines have been analyzed (see Sec. II C-3).

The hf interactions for the Sb and P donors were determined only for the magnetic field directions along

[29] Experimentally the two [110] axes cannot be distinguished from each other, i.e., we cannot find out from the experiment whether the hf interaction with the field in the (110) plane containing the 331 sites is smaller or larger than when it is in the (110) plane at right angles to it (i.e., containing the 551 sites).

TABLE I. The experimental and theoretical values of the hf interaction of the donor electron with the Si^{29} nuclei. The theoretical values are based on the theory of Kohn and Luttinger.[a]

		Line A (400)			Line B (440)			Line C (333)		Line D (555)		Line E (111)		(444)
		$a/2$ Mc/sec	$b/2$ Mc/sec	$b'/2$ Mc/sec	$a/2$ Mc/sec	$b/2$ Mc/sec	$b'/2$ Mc/sec	$a/2$ Mc/sec	$b/2$ Mc/sec	$a/2$ Mc/sec	$b/2$ Mc/sec	$a/2$ Mc/sec	$b/2$ Mc/sec	$a/2$ Mc/sec
As	Experiment	3.86	0.023	0.020	3.00	0.052	−0.006	2.04	0.004	1.29	0.012	0.80	0.55	
	Theory: $k_0/k_{max}=0.83$	4.50			1.51			2.05		1.38		1.41		0.49
	$k_0/k_{max}=0.86$	5.01			2.01			1.48		1.15		0.92		0.92
$E_i=0.050$ ev	$k_0/k_{max}=0.89$	5.48			2.56			0.95		0.82		0.54		1.38
P	Experiment	2.98	0.017	0.014	2.26	0.028	$\cdots$	1.64	<0.004	1.13	0.010			
	Theory: $k_0/k_{max}=0.83$	3.74			1.33			1.80		1.30		1.08		0.45
	$k_0/k_{max}=0.86$	4.16			1.77			1.28		1.08		0.72		0.82
$E_i=0.045$ ev	$k_0/k_{max}=0.89$	4.55			2.20			0.80		0.77		0.44		1.25
Sb	Experiment	3.10	0.015	0.008	1.83	0.024	$\cdots$	1.39	<0.004	1.01	0.008	0.60	0.12	
	Theory: $k_0/k_{max}=0.83$	2.88			1.03			1.56		1.18		0.73		0.38
	$k_0/k_{max}=0.86$	3.22			1.49			1.02		0.97		0.47		0.72
$E_i=0.040$ ev	$k_0/k_{max}=0.89$	3.52			1.85			0.64		0.69		0.28		1.08

[a] See reference 6.

the three principal crystalline axes. Once the site is identified this procedure is sufficient to obtain values for a_l, b_l, b_l' which are tabulated in Table I.

(b) *Line B.*—Having obtained from line A a rough value of k_0/k_{max} one is now in a position to predict from Fig. 8 the remaining lines. The Si^{29} nucleus which has the second largest hf interaction is expected according to Fig. 8 to be at the 440 site (ninth nearest neighbor). As in the case of line A one first determines from simple symmetry arguments the direction of the principal axis of the anisotropic hf interaction. An inspection of the crystal lattice (see Fig. 7) shows that one axis must lie in the (110) plane (see shaded area of Fig. 7) but not necessarily along the line connecting

FIG. 10. Hf interaction of the donor electron in As-doped silicon with the Si^{29} nuclei at the 440 site (see Fig. 8). The magnetic field is rotated in the (110) plane of the crystal, angles are measured from the [100] direction. The full lines represent the theoretical fit given by Eq. (11). Note that the principal axis makes an angle α with the [110] direction.

the 440 site with the donor. The reason is that the nearby 133 site can disturb the electronic wave function sufficiently to shift the axis. The angle α that the axis makes with the line connecting the 440 site with the donor is then an additional parameter that can be determined from experiment. Again one has no reason to assume that the hf interaction will have axial symmetry. It can be seen, however, from symmetry considerations that the second axis must be along the [110] (in Fig. 7 the [011]) direction.

Figure 10 shows the experimental points and the theoretical fit for As-doped silicon. The parameters chosen for the theoretical curves are

$$\alpha=23°, \quad \tfrac{1}{2}a_l=3.00 \text{ Mc/sec}, \quad \tfrac{1}{2}b_l=0.052 \text{ Mc/sec},$$

$$\tfrac{1}{2}b_l'=-0.006 \text{ Mc/sec}.$$

From these values we see that the 440 site is almost axially symmetric, the axis being tilted[30] towards the [111] axis by 23°. This angle was found to be 19° for phosphorus and 15° for antimony-doped silicon. The deviation from axial symmetry for those two centers was too small to be determined from measurements along the 3 principal directions. Although the theoretical fit for this line is not perfect there seems to be little doubt as to the symmetry of the center. It should be added however that any site lying in the (110) plane (e.g., 331, 551) may have such a symmetry. The final choice of the 440 site was based on Fig. 8.

(c) *Line C and D.*—We treat line C and D together since they are both due to centers having [111] symmetry. The [111] direction is the only one that must exhibit axial symmetry and should be therefore easily fitted with a theoretical curve. Unfortunately it turns out that the anisotropic part of the lines is small and line C splits only in the [111] direction (see Fig. 11) and merely broadens in the [110] direction. This behavior however is sufficiently distinct from lines of other symmetries to assign it to the [111] direction.

[30] Again from the experimental results one cannot deduce whether the axis tilts towards the 331 site (as indicated in Fig. 7) or away from it.
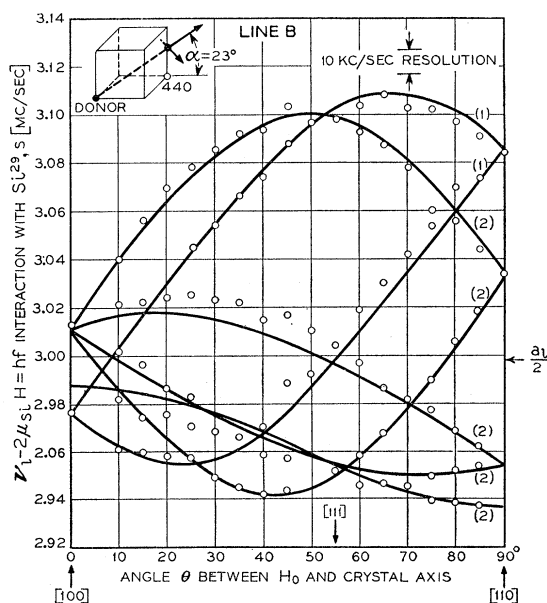
Line D is resolved in both directions and was fitted with a theoretical curve assuming $\frac{1}{2}a_l = 2.04$ Mc/sec, $\frac{1}{2}b_l = 0.004$ Mc/sec. The fits for both lines are illustrated in Fig. 11 and the values of $\frac{1}{2}a_l$ and $\frac{1}{2}b_l$ are tabulated in Table I.

The precise assignment of the lines is considerably more difficult. Each of the lines may be due to the 333, 444, or 555 site. From symmetry arguments alone one cannot of course distinguish between these sites and neither can one eliminate any of them by calling on Fig. 8; all three sites should have a comparable hf interaction for k_0/k_{max} in the neighborhood of 0.84–0.86. One has to look therefore for other features that might distinguish between the three lines. One of them is the number of equivalent sites. There are eight 444 sites but only four 333 and four 555 sites. From the relative amplitudes of line C and D to be discussed in Sec. II C-2e one can exclude the 444 site and is left therefore with the two choices corresponding to the 333 and 555 assignments. The distinguishing feature of these two sites is their different distance from the donor nucleus. One would expect therefore that the ratio a_{333}/a_{555} would be large for electrons having a more tightly bound wave function, i.e., for donors with a larger ionization energy. Thus one expects

$$(a_{333}/a_{555})_{As} > (a_{333}/a_{555})_{P} > (a_{333}/a_{555})_{Sb}. \quad (12)$$

This inequality should be independent of k_0/k_{max} although the absolute value of the ratios will depend on k_0/k_{max}. Table II summarizes the ratios of the observed hf interactions a_C/a_D together with the theoretical ratios a_{333}/a_{555} assuming $k_0/k_{max} = 0.85$. A comparison of the corresponding ratios leads us then to identify line C with site 333 (seventh nearest neighbor) and line D with site 555 (twenty-third nearest neighbor).

(d) *Line E.*—Referring to Fig. 4 one sees an additional line in the [111] direction which is not observable in the [100] and [110] directions. A closer examination of this line indicates that it must be a fragment of a line with a large anisotropic hf interaction. The circles in Fig. 12 show the experimental position of this fragment for $35° < \theta < 75°$. (Note the compressed scale of the ordinate in comparison to Figs. 9, 10, 11). The entire line cannot be traced out since most of it merges with other lines at lower frequencies. The fragment itself disappears even before coinciding with other

TABLE II. Identification of lines C and D by comparing the ratios of the observed hf interactions a_C/a_D with the theoretical values a_{333}/a_{555}. Since the ratios increase with increasing ionization energy one is led to believe that line C is due to a nearer Si^{29} nucleus than line D.

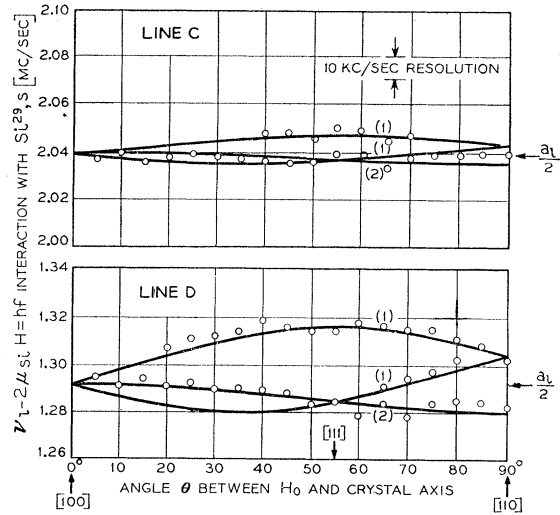| Donor	Ionization energy [ev]	a_C/a_D (exp.)	a_{333}/a_{555} (theory) ($k_0/k_{max} = 0.85$)
As	0.049	1.58±0.01	1.35
P	0.044	1.45±0.01	1.25
Sb	0.039	1.38±0.01	1.13

FIG. 11. Hf interaction of the donor electron in As-doped silicon with the Si^{29} nuclei at the 333 site (line C) and 555 site (line D). The magnetic field is rotated in the (110) plane of the crystals (see Fig. 8), angles are measured from the [110] direction. The full lines represent the theoretical fit given by Eq. (6).

lines. Because of the large anisotropy of the line its sensitivity to angular variations is greatly enhanced at angles off the [111] direction and may account for its premature disappearance.

Since the largest hf interaction always occurs along the axis of symmetry of a center one may assume that line E has a [111] symmetry. In view of the large anisotropy, discussed more fully in Sec. II C-2f, it seems clear that line E is due to the [111] site (nearest neighbor). The amplitude of line E is consistent with this assignment. (See next section.) In view of the large dipolar interaction the silicon nucleus will not point along the external magnetic field but will be tilted toward the [111] direction. This results in a small correction term to be added to Eq. (6), which becomes

$$hv_l^{\pm} = \left| \frac{-\mu_{Si}}{I_{Si}}H \pm \frac{a_l}{2} \mp \frac{b_l}{2}(1 - 3\cos^2\theta) \right.$$
$$\left. + \frac{9}{2}\left(\frac{b_l}{2}\right)^2 \frac{\cos^2\theta \sin^2\theta}{-2\mu_{Si}H \pm \frac{1}{2}a_l \mp \frac{1}{2}b_l(1 - 3\cos^2\theta)} \right|. \quad (13)$$

The theoretical fit of the [111] fragment with the observed experimental points is illustrated in Fig. 12. The parameters chosen were: $\frac{1}{2}a_l = 0.80$ Mc/sec, $\frac{1}{2}b_l = 0.55$ Mc/sec.

In P-doped silicon the line E was not found, presumably, because it coincided with the lower frequency lines.

(e) *Relative amplitudes of the lines.*—As pointed out in Sec. II(C)2e the relative amplitudes of the ENDOR lines should serve as an additional check on the proper identification of the lines. The problem is analyzed in
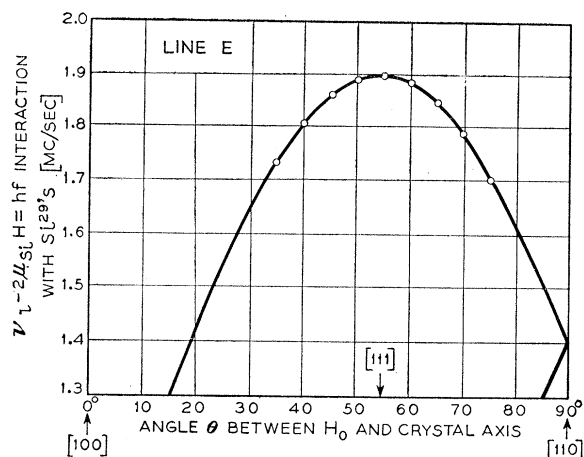
FIG. 12. Part of the hf interaction of the donor electron in As-doped silicon with the nearest neighbor Si^{29} nuclei (111 sites). The magnetic field is rotated in the (110) plane of the crystal (see Fig. 7), angles are measured from the [110] direction. The full lines represent the theoretical fit given by Eq. (13).

Appendix B where it is found that the relative amplitudes depend on the setting of the magnetic field H with respect to the center of the electron spin resonance line. If the value of H corresponds to the center of the line the relative amplitudes $A_l(0)$ are proportional to the number of equivalent silicon sites (n_l) times a weighting factor $h^*(\frac{1}{2}a_l)$ defined in Appendix B. Table III summarizes the experimental and predicted relative amplitudes normalized to line A. The experimental values were obtained for As-doped silicon ($\sim 8 \times 10^{16}$ As/cm³). For the lines that show a resolved anisotropic hf interaction the amplitudes were obtained by adding up all the individual peaks corresponding to the same line. This is illustrated in Fig. 13 which shows line B in arsenic-doped silicon with the magnetic field pointing along the [111] direction. The line is split into three components with an amplitude ratio 2:1:1 as expected from this site when H points along the [111] direction (see Fig. 10). The dotted lines indicate the base lines from which the amplitudes of the individual peaks are measured. In the case of line E, the observed amplitude was multiplied by four in accordance with its identification as a [111] fragment.

In view of the simplifying assumptions made in arriving at $A_l(0)$ the agreement shown in Table III is considered fair. The largest discrepancy occurs for line D which is 35% smaller than its predicted value. There are several possible explanations which may account for this discrepancy. Because of the smallness of the hf interaction of this line the spin packets that are responsible for it are only 0.4 oersted removed from the saturated part of the electron spin resonance line and therefore may themselves be partially saturated. Furthermore because of the relatively large distance of this site from the donor atom, it is the most likely one to be broadened by interactions with neighboring arsenic donors which would also reduce its amplitude.
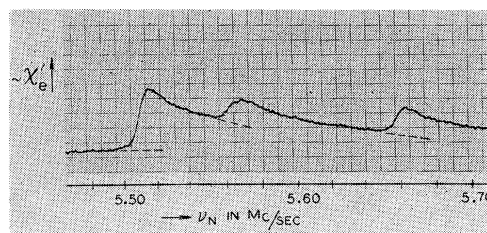

FIG. 13. Expanded trace of line B in As-doped silicon (see Fig. 4) with the magnetic field along the [111] direction. The dotted lines represent the base lines from which the relative amplitudes are measured. Note from Fig. 10 that the expected ratio of amplitudes is 2:1:1 in approximate accord with the above trace. (8×10^{16} As/cm³, $T = 1.25°$K, $H_0 \sim 3050$ oersteds.)

It should be noted that a better agreement would be obtained if for line D we choose $n_l = 3$ instead of 4. However, there are *no* silicon sites which have less than four equivalent sites so that the assignment 555 is the most plausible one in spite of the observed amplitude discrepancy.

(*f*) *Note on the anisotropic hf interaction.*—So far we have considered the anisotropic hf interaction only as an aid in identifying the ENDOR lines. An exact knowledge of the donor wave function should enable one also to predict the magnitude of the anisotropic component. An attempt to predict the dipolar part of the interaction was made by B. Mozer.[31] He used the Kohn-Luttinger wave function simplified by a tight binding approximation and obtained an equation similar to Eq. (6) where the cosines were replaced by sine functions. This expression failed completely to account for the relative amplitudes of the observed anisotropies. Anderson[32] suggested that polarization effects might play a predominant part in the anisotropic hf interaction. This effect would be more pronounced for the nearest neighbors which see the unscreened positive charge. It presumably also accounts for the large anisotropy of the [111] site.

It should be also noted that s- and p-functions alone must result in an axially symmetric hyperfine interaction. The observation of the large deviations from axial symmetry (see line A) must therefore arise from higher angular momentum wave functions.

(3) Determination of k_0/k_{max}

Table I summarizes the experimental results and the predicted values based on the theory of Kohn and Luttinger.[6] The theoretical values were obtained for As from Fig. 8 and for the other two donors from similar plots, assuming three different parameters for k_0/k_{max}. They are all based on the value of $\eta = 186$.[23] A comparison of these values with the experimental ones shows that one cannot fit the data with a unique k_0/k_{max} as would be expected from a perfect theory. Line C and D would be best fitted with an average

[31] B. Mozer (private communication).
[32] P. W. Anderson (private communication).

TABLE III. Comparison of the experimental and predicted ENDOR amplitudes assuming the assignment as indicated. Both $A_l(0)$ and the experimental values are normalized to line A.

Line site	A 400	B 440	C 333	D 555	E 111
n_l	6	12	4	4	4
Predicted amplitudes, $A_l(0) = n_l h^*(a_l/2)$	1.0	2.7	1.0	1.1	1.1
Experimental amplitudes	1.0	2.5	1.0	0.7	0.9

TABLE IV. Hf interactions of the electron with different donor nuclei. The accuracy is required in connection with nuclear structure problems.

Donor	a_D (Mc/sec)	$|\Psi(0)|^2$ (cm^{-3}) Experiments	$|\Psi(0)|^2$ (cm^{-3}) Theory
Sb^{121}	186.802±0.005[a]	1.18×10^{24}	...
Sb^{123}	101.516±0.004[a]	1.18×10^{24}	...
P^{31}	117.53 ±0.02[b]	0.43×10^{24}	0.4×10^{24}[d]
As^{76}	198.35 ±0.02[c]	1.73×10^{24}	...

[a] See reference 17.
[b] Taking this new value of a (P^{31}) one obtains g_I(P^{32}) = −2.526 which is within the experimental error of the previously quoted value (reference 34).
[c] This value is to be compared with (198.42±0.04) Mc/sec reported by J. W. Culvahouse and F. M. Pipkin [Phys. Rev. 109, 1423 (1958)].
[d] See reference 6.

$k_0/k_{max} = 0.84$ and 0.85, respectively, line B with $k_0/k_{max} = 0.9$, line A with k_0/k_{max} around 0.8. As expected from Kohn and Luttinger's theory, which was developed for shallow donors, the worst agreement is observed in As which is the most tightly bound donor. The theory is also expected to become less reliable the closer one gets to the donor nucleus. This point is clearly exhibited by line A which shows the poorest agreement and is believed to be due to the closeness of the 400 sites to the donor. The relatively good agreement of the position of the nearby [111] sites seems somewhat fortuitous. By averaging all the values of $k_0/k_m r_x$ required to fit the data we arrive at[33,34]

$$k_0/k_{max} = 0.85 \pm 0.03.$$

It should be noted that even if the assignment of line C and D should be reversed or even if either of them should be assigned to the 444 site, the value of k_0/k_{max} would still stay within the above uncertainty limits. These limits do not of course represent an experimental error but are based on the discrepancy of experiment with theory. An improvement in theory would lead to a more accurate determination of k_0/k_{max} and also of η. At present our limits on η are larger than the ones quoted by Shulman and Wyluda.[23]

With the value of $k_0/k_{max} = 0.85$ the theory of Kohn and Luttinger predicts *all* the observed *isotropic* hf interaction to within about 50%. However, the attempt by Mozer[31] based on the simplified wave function of Kohn and Luttinger failed completely to account for the *anisotropic* part.

The value of k_0/k_{max} estimated by Phillips from the infrared work of Haynes et al.[35],* and the value obtained by McFarland[36] are consistent with the above value.

(4) Hf Interaction with the Donor Nuclei

The values of the hf interactions of the electron with different donor nuclei reported by Fletcher et al.[4,5] were

sufficiently accurate for "solid state" purposes. However, in view of the recent applications of donor resonances to nuclear structure problems[37,17,38] more accurate determinations of a_D are required. Table IV summarizes the results obtained by the ENDOR technique at 1.25°K. In computing a_D from the experimentally observed transitions appropriate corrections[17,39] to Eq. (5) were made to account for the fact that the experiments were not performed in the extreme high-field region.

D. The Electron Spin Resonance Line Shape

(1) The Experimentally Observed Line Shape

In most electron spin resonance experiments one encounters electron spin-lattice relaxation times that are short in comparison to the time it takes to sweep through the resonance line or even through a single spin packet. In such "slow passage"[10] cases the line shape (or its derivative if a modulation technique is used) would be a faithful reproduction of the distribution of local fields as seen by the individual spin packets. The importance of passage effects on the line shape in electron spin resonance experiments was first pointed out by Portis.[40,41] In the early experiments[42] such effects were not appreciated and were at least in part responsible for the erroneous conclusions[43] reached. In the present study the relaxation times may be as long as an hour (see Part II) and in order to observe a signal one has to look at the dispersion mode under so-called "fast adiabatic passage"[10] conditions. Before comparing the observed line shape with theory one has to investigate how the experimentally determined line shape is expected to differ from the distribution of resonance fields of the spin packets.

[33] The preliminary value that we quoted at the Radio and Microwave Spectroscopy Conference, Durham, North Carolina, 1957 (ONR Report ACR-31) was $k_0/k_{max} = 0.86$.
[34] An account of this work was given at the International Conference on Semiconductors, Rochester, New York, 1958, and published in J. Phys. Chem. Solids 8, 486 (1959).
[35] Haynes, Lax, and Flood, Bull. Am. Phys. Soc. Ser. II, 3, 31 (1958).
* Note added in proof.—The original interpretation of the infrared data seems at present doubtful. [See Haynes, Lax, and Flood, J. Phys. Chem. Solids 8, 392 (1959).]
[36] Macfarland, McLean, Quarington, and Roberts, Phys. Rev. 111, 1245 (1958).

[37] F. M. Pipkin and J. W. Culvahouse, Phys. Rev. 106, 1102 (1957).
[38] Feher, Fuller, and Gere, Phys. Rev. 107, 1462 (1957).
[39] N. F. Ramsey, Molecular Beams (Clarendon Press, Oxford, 1956).
[40] A. M. Portis, Phys. Rev. 100, 1219 (1955).
[41] A. M. Portis, Technical Note No. 1, Sarah Mellon Scaife Radiation Laboratory, University of Pittsburgh, November 15, 1955 (unpublished).
[42] A. Honig, Phys. Rev. 96, 234 (1954).
[43] A. Honig and J. Combrisson, Phys. Rev. 102, 917 (1956).

The passage conditions under which the line shapes were determined are discussed in Appendix A. A 100-cps field modulation was used with an amplitude large in comparison to the microwave field H_1 but small compared to the line width ΔH. Each spin packet was traversed under adiabatic fast passage conditions. The magnetic field was slowly varied in such a way that for each value of H_0 a steady state condition was reached. This was achieved by illuminating the sample (see Part II) and thereby reducing the relaxation time. The line shape under the above conditions is given by Eq. (38).

Figure 14 shows the trace of one of the experimentally observed resonance lines in phosphorous-doped silicon (1.5×10^{16} P/cm³) at 1.25°K. The dotted line indicates the theoretical curve using Eq. (38) normalized to the half-power points. The parameters used are: $2\Delta H = 2.5$ oersteds and $\Delta H/H_1 \approx 300$. It is shown in the Appendix that with this value of β the observed line width is $\sim 10\%$ larger than that corresponding to the true distribution of spin packets. This correction was applied to the observed line widths (ΔH_{obs}) which are summarized in Table V, together with the predicted widths (ΔH_{pred}) discussed in the next section. The good fit of the theoretical line shape with the experimental trace gives us some confidence that the assumption of a Gaussian distribution is justified. An additional confirmation of the validity of this assumption is provided by the ratio

$$\Gamma = (M_4)/(3M_2)^2, \qquad (14)$$

which should be unity for a Gaussian line shape and should deviate only by a negligible amount from unity if the shape is given by Eq. (38). Here M_4 is the fourth and M_2 the second moment of the line. Both moments were determined graphically from traces like the one shown in Fig. 14.

Table V also shows the results obtained using an isotopically enriched Si²⁸ sample.[44] It has a reduced line width and the shape deviates appreciably from a Gaussian as exhibited by the large value of Γ. Also the deviations for As from a Gaussian are larger than those
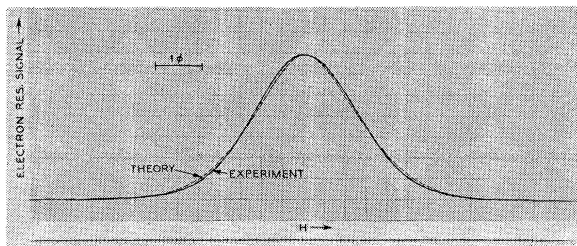

F Fig. 14. Electron spin resonance line shape in phosphorus-doped silicon (1.5×10^{16} P/cm³, $T = 1.25$°K, $H_0 \simeq 3200$ oersteds). Magnetic field modulation was used and the microwave bridge was sensitive to the dispersion mode. The dotted line represents the expected shape as discussed in Appendix A-2.

[44] Feher, Gordon, Gere, and Thurmond, Phys. Rev. 109, 221 (1958).

for Sb and P. Both of these effects are explained in the next section.

As shown in Appendix A-1, one would expect the shape of the resonance signals to be the same if one traverses the lines without magnetic field modulation under adiabatic fast passage conditions. In practice it was found however that the line shapes observed under these conditions were asymmetric and gave a 5–10% larger line width. This presumably is due to a spin diffusion process discussed in Part II (see also Appendix A-4). Because of the observed asymmetry this mode of operation was abandoned in the study of line shapes.

It should be noted that the experimental errors quoted in Table V of ΔH and Γ are based on the reproducibility of data obtained on the same sample under similar conditions. More work needs to be done in order to establish the effect of spin diffusion on the line shape. We have assumed the complete absence of spin diffusion in arriving at the theoretical line shape.

(2) The Predicted Line Shape

Since the electron spin resonance line width arises from the hf interaction of the electron with the Si²⁹ nuclei one should be able to predict the line width from the hf interactions determined from the ENDOR experiments. One would of course need to know all the interactions in order to reconstruct the exact line shape. However, as will be shown presently about 80% of the line width arises from the four largest hf interactions (lines A, B, C, D summarized in Table I). The hf interactions of the rest of the Si²⁹ "shells" may then be calculated from the theory of Kohn and Luttinger.[6]

The resonance field of a donor electron having its lth lattice site occupied by a Si²⁹ is shifted by $\pm a_l$, where a_l is defined by Eq. (3). Hence one can write for the second moment M_2 of the line

$$M_2 = \Delta H_{rms}^2 = \sum_{l=0}^{\infty} f n_l (a_l/2)^2, \qquad (15)$$

where n_l is the number of equivalent Si sites[45] in the lth "shell" and f is the fractional abundance of Si²⁹ ($f = 0.047$). $f n_l$ is then the probability of having the lth lattice site occupied with a Si²⁹. Let us divide the summation into two parts:

$$\Delta H_{rms}^2 = \sum_{l=exp} f n_l (a_l/2)^2 + \sum_{l=1, l \neq exp}^{24} f n_l (a_l/2)^2, \qquad (16)$$

where the first summation includes only the first four largest hf interactions as determined by the ENDOR technique and the second summation extends over the first 24 nearest Si²⁹ shells excluding the sites that were taken into account in the first summation. The different a_l's in the second sum were obtained by taking k_0/k_{max}

[45] The nonequivalence due to the anisotropic part of the hf interaction can be neglected in this discussion.

TABLE V. Line width and moments of the electron spin resonance line for different donors. The experimental widths are corrected for passage effects (see Appendix A). The ratio $M_4/3M_2{}^2$ should be unity for a Gaussian line. The predicted widths are derived from the hf interactions. Note that the half-width at the half-power point ΔH is 1.18 times the second moment for a Gaussian line.

Donor	Concentration	$2\Delta H_{obs}$ (oersteds)	$2\Delta H_{cor}$ (oersteds)	$2\Delta H_{pred}$ (oersteds)	$\Gamma = M_4/3M_2{}^2$
Sb	$2.5\times10^{16}/\text{cm}^3$	$2.6\ \pm0.1$	2.3	2.3	1.0 ± 0.1
P	$1.5\times10^{16}/\text{cm}^3$	$2.8\ \pm0.1$	2.5	2.5	1.0 ± 0.1
As	$1.8\times10^{16}/\text{cm}^3$	$3.2\ \pm0.1$	2.9	3.1	1.3 ± 0.1
P in isotopically purified Si$\approx$99.88% Si^{28}	$4\ \times10^{16}/\text{cm}^3$	0.24 ± 0.02			1.8 ± 0.1

$=0.85$ and calculating the hf interactions from Eq. (9) as was done in the construction of Fig. 8. Since the donor electron wave function falls off exponentially the inclusion of only the first 24 shells seems adequate. The contribution of the second sum to ΔH_{rms} is only about 20%. Values of the line widths for different donors calculated from Eq. (16) are listed in Table V.

The electron spin resonance line shape has been investigated by Kohn[25,24] who showed that if the electronic wave function extends over a very large number of Si^{29} sites the line shape can be represented by a Gaussian function. This is a fair approximation for shallow donors in silicon and is born out by experiment as judged from the values of Γ listed in Table V.

In the case of the isotopically enriched Si^{28} sample the number of Si^{29} nuclei with which the electron interacts is greatly reduced and the line shape is expected to deviate from a Gaussian. The experimentally determined value of $\Gamma = 1.9$ shows that this is indeed the case. By a similar argument one concludes that the largest deviation of Γ from unity should occur for the tightest bound center which is arsenic. For this donor Kohn[25] calculates a value of $\Gamma \approx 1.25$ which is in good agreement with experiment.

It is interesting to note that before the double resonance data were available Kohn[25,24] calculated the line widths for different values of k_0/k_{max}. The best agreement with the experimental line-width results was obtained for $k_0/k_{max} = 0.70\pm0.25$ which is consistent with the more precise value of 0.85.

In all the foregoing discussions it was assumed that the Si^{29} spins point with equal probability along or opposite to the magnetic field. This results in a symmetrical line having no odd moments. If one were to polarize the Si^{29} nuclei (e.g., by an Overhauser effect) one should observe both a shift and an asymmetry of the line. No such effect was observed. The asymmetry noted under certain passage conditions is presumably due to a different mechanism as pointed out in the preceding section.

E. Electronic g-Values

(1) Experimental Results

The original experiments of Fletcher et al.[5] indicated that the g-values of all the donors were the same and equal to the g-value of the conduction electrons in silicon.[2] By improving the precision of the measure-

ments we have determined the difference in g-values between the different donors and the conduction electrons. By conduction electrons we mean, here, the charge carriers in heavily doped silicon, in our case 3×10^{18} P/cm^3. Such a sample exhibits a single narrow homogeneously broadened resonance line similar in its behavior to the resonance lines obtained from conduction electrons in metals.

The experiments were performed by sandwiching two samples together. One was doped with the donor whose g-value was to be measured and the other (0.25 mm thick) contained the heavy phosphorus doping. Figure 15 shows the experimental trace obtained on such a compound sample. In this case one silicon wafer was double-doped $\approx5\times10^{15}$ As/cm^3 and $\approx5\times10^{15}$ P/cm^3. The trace clearly shows the difference in line shape between a slow passage (derivative of a dispersion line) obtained from the conduction electrons and an adiabatic fast passage as discussed in Appendix A-2. The upper trace in Fig. 15 shows the magnetic field markers obtained from a proton sample. In the determination of the g-values the magnetic field sweep was slowed down by a factor of 20 and the gain increased by 20 db. The sample was illuminated in order to reduce the relaxation time (see Part II) and to get symmetrical lines. The reproducibility of determining their centers was within a few millioersteds. The g-value of the conduction electrons was found to be

$$g_{C.E.} = 1.99875 \pm 0.00010. \tag{17}$$

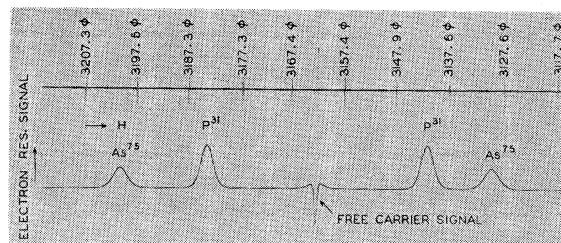The experimental error was estimated from the uncertainty in the field difference between the proton sample

FIG. 15. Electron spin resonance signals from two silicon samples. The central line is due to conduction electrons in a heavily doped sample $(3\times10^{18}$ P/cm$^3)$. The sample with $\sim5\times10^{15}$ As/cm^3 and $\sim5\times10^{15}$ P/cm^3 exhibits hf structure due to localized electrons. Field markers are derived from a proton sample. Note the difference in line shapes characteristic of "slow" and "adiabatic fast" passages.[10] (See Appendix A.) $(T = 1.25°K, \nu_e = 8845.3$ Mc/sec.)

and the silicon samples. This uncertainty arises from variable field gradients ($\pm$30 millioersteds) and demagnetizing fields presumably due to paramagnetic impurities embedded in the microwave cavity walls. The latter point was ascertained by rotating the magnetic field with respect to the cavity.[46] Because of the noncylindrical shape of the (glass) cavities used, apparent "g-shifts" of $\approx 3\times 10^{-5}$ were observed. In a brass cavity this effect was found to be larger by about a factor of four. The originally reported large anisotropy in the g-values[5] was presumably due to ferromagnetic inclusions[47] in the cavity walls.

All the donor g-values (g_D) are referred to the g-value of the conduction electrons ($g_{C.E.}$). This eliminates the above mentioned uncertainties and increases the relative accuracy by about one order of magnitude. Since we are not in the extreme high-field region the g_D's were obtained by using the exact Breit-Rabi formula[39] [instead of Eq. (4)] rewritten for our purposes in the more convenient form[48]

$$g_T{}^2\left[\left(\frac{\mu_0 H}{a_D}\right)^2 - \frac{1}{4}\left(\frac{\mu_0 H}{\nu_e + g_I \mu_0 H}\right)^2\right] + 2g_T m_D\left(\frac{\mu_0 H}{a_D}\right)$$

$$+ (I+\tfrac{1}{2})^2 - \left(\frac{\nu_e + g_I \mu_0 H}{a}\right)^2 = 0, \quad (18)$$

where $g_T = g_D + g_I(m/M)$, m/M is the electron-nuclear mass ratio, m_D is the nuclear magnetic quantum number corresponding to the transition under consideration, a_D the hf interaction as listed in Table IV and μ_0 is the Bohr magneton [1.39968 (Mc/sec)/oersted].

The results for $g_D - g_{C.E.}$ are listed in Table VI.

It is worth pointing out that the silicon sample with 3×10^{18} P/cm^3 used above meets all the requirements of a useful field calibration sample ("g-marker"): (1) It exhibits a narrow, symmetric resonance line. (2) The line is isotropic.† (3) The sample is stable for an indefinite period. (4) Its magnetization even at 1°K is low enough so that corrections due to demagnetizing fields are negligible. By comparison, the usual g-marker diphenyl picryl hydrasyl[49] falls short at low temperatures in all four respects. The amount of doping used seems to be near the optimum to give the minimum line width. If one reduces the number of phosphorus

---

[46] The g-value of the conduction electrons is isotropic because of the short collision time of the electrons. The g-value of the donor electron should be isotropic because of symmetry considerations. The measurements were made with H_0 along the [110] direction.

[47] R. C. Fletcher (private communication).

[48] This corresponds to Eq. (4) of reference 17 where due to a misprint the first bracket was not squared.

† *Note added in proof.*—In view of the anisotropic line width found in the resonance absorption of shallow donors in germanium [Feher, Wilson, and Gere, Phys. Rev. Letters 3, 25 (1959)] the isotropy of the line width in silicon was reinvestigated. Within the experimental accuracy ($\simeq 2\%$) no variation in line width with angle was detected.

[49] Holden, Kittel, Merritt, and Yager, Phys. Rev. 77, 147 (1950).

TABLE VI. Difference between the g-value of donor electrons (g_D) and the unbound conduction electrons ($g_{C.E.}$). The latter is obtained from a heavily doped phosphorus sample (3×10^{18} P/cm^3, $T = 1.25°$K; $\nu_c \simeq 9000$ Mc/sec). Note that the difference increases with increasing ionization energy E_i of the donor.

Donor	E_i (mv)ᵃ	$g_D - g_{C.E.}$
Sb	39	$-(1.7\pm 0.1)\times 10^{-4}$
P	44	$-(2.5\pm 0.1)\times 10^{-4}$
As	49	$-(3.8\pm 0.1)\times 10^{-4}$

ᵃ See reference 27.

impurities, the electrons are not as free to move through the crystal and therefore average out the local hyperfine fields less effectively, which results in a broader resonance line. This behavior is illustrated in Fig. 16 which shows the transition from a completely localized center[15] [Fig. 16(a)] to a free carrier [Fig. 16(d)] as was used for the g-marker. A reduction in the number of impurities from 3×10^{18} P/cm^3 to 1.5×10^{18} P/cm^3 increases the line width at 1.25°K from 0.5 oersted to 1.2 oersteds, although the g value still stays within the above quoted limits. On the other hand an increase in the donor concentration increases the collision frequency of the electrons which again broadens the line. In addition it becomes difficult to make a highly conducting sample small in comparison to a skin depth. If this condition is not satisfied one obtains an asymmetric metal-like resonance line[50] which would not be well suited for a g marker.

2. Discussion of the Results

The deviation of the observed g value of the conduction electrons from the free electron value of 2.0023 is due to spin-orbit coupling and is of the order $\Delta g \approx \lambda/\Delta E$,[51] where λ is the spin-orbit coupling constant estimated by Elliott[51] to be ~ 100 cm^{-1}. From the observed g shift one obtains then for ΔE, the separation of the nearest band that is admixed, a value of ~ 3.5 ev. This represents only an approximate estimate; an exact calculation would have to take into account the admixture of several bands and has not been carried out so far.

In the last section it was found that the deviations of the donor g value (g_D) from the conduction electron g value ($g_{C.E.}$) increase with increasing ionization energy. This is not surprising since one would expect the largest deviations for the most tightly bound donor. In the limit of very small ionization energies g_D should approach the value of $g_{C.E.}$. The relative g values of the donors could be obtained if one knew the p-part of the wave function at all the lattice points. The experimental values of b provide such information [see Eq. (3) and Table I] for a limited number of sites. It seems, however, that the remaining sites contribute

---

[50] G. Feher and A. F. Kip, Phys. Rev. 98, 337 (1955); F. J. Dyson 98, 349 (1955).

[51] R. J. Elliott, Phys. Rev. 96, 266 (1954).

significantly to the g shift and must be taken into account. Calculations along these lines are presently being performed by Abrahams.[52]

The contribution to the g shift from the spin-orbit coupling with the impurity atom itself seems to be very small. This may be concluded from the fact that no large change in the value of $g_D - g_{C.E.}$ is observed between P and Sb whose atomic spin orbit couplings differ by more than an order of magnitude.

III. MISCELLANEOUS CENTERS

Besides the shallow donors As, P, Sb, discussed in the previous sections several other centers were found to exhibit a paramagnetic resonance signal. The experiments on these centers are briefly summarized in this section. The centers to be discussed were investigated in considerably less detail than As, P, Sb. This work should, therefore, not be considered as completed but merely as a basis for further experiments that are required to determine the detailed electronic structure of these centers.

A. Bismuth

Bismuth belongs to the Group-V elements and forms a donor in silicon with an ionization energy of 0.068 ev.[27] Since its ionization energy is much larger than that of the other Group-V elements (As, P, Sb), the theory of Kohn and Luttinger is expected to be less applicable to this center. This is the reason why the results on Bi were not lumped together with those of the other three donors. The experiments were performed on a sample having a Bi concentration of $\sim 2 \times 10^{16}$ Bi/cm^3. The line width, g value, and hyperfine splitting with the Bi^{209} ($I = 9/2$) nucleus were found from the ordinary resonance spectrum at 1.25°K and ~ 9000 Mc/sec to have the values

$$\Delta H = 4.5 \pm 0.2 \text{ oersteds,}$$

$$g = 2.0003 \pm 0.0001,$$

$$a_D = 1475.4 \pm 0.1 \text{ Mc/sec;}$$

therefore,

$$|\Psi(0)|^2 = 1.4 \times 10^{25} \text{ cm}^{-3}.$$

The larger line width is to be expected from the larger ionization energy of the center (see Sec. IID). It is of interest to note that the g shift does not follow the extrapolated monotonic increase with increasing ionization energy that is observed for the Sb, P, and As donors. The zero-field hf splitting $\Delta\nu$ lies in the microwave region and has a value

$$\Delta\nu = a(I + \tfrac{1}{2}) = 7377 \text{ Mc/sec,}$$

The large splitting makes it possible to use this center for a two-level zero-field maser.[53,44]
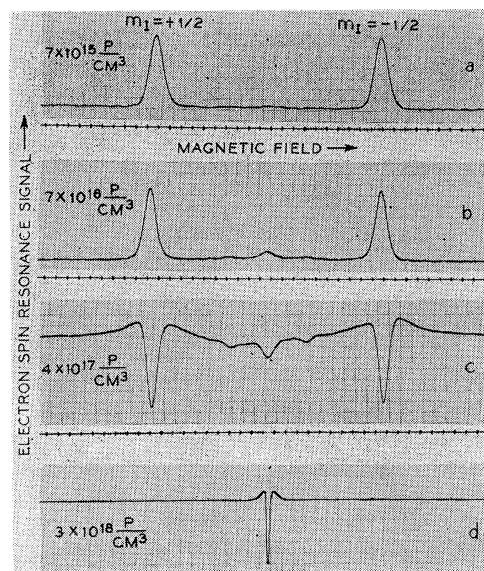

FIG. 16. Electron spin resonance signal from silicon doped with varying amounts of phosphorus. The range covers the transition from localized centers (a) to free carriers (d) as were used for the g-marker. For concentrations between these two extrema the observed resonance signal is due to clusters of phosphorus atoms[15] (b,c). This region marks the beginning of the impurity band conduction process. The different line shapes are a result of the change in relaxation times which cause the transition from "adiabatic fast" to "slow" passage conditions[10] (see Appendix A) ($T = 1.25$°K, $\nu_e \cong 9000$ Mc/sec).

B. Lithium

Lithium forms a donor in silicon[54] with an ionization energy of 0.033 ev. The samples used in our experiments were prepared[55] by diffusing $\sim 3 \times 10^{16}$ Li/cm^3 into high resistivity silicon. The electron spin resonance signal of this center was first observed by Honig and Kip[56] who reported a single resonance line at ~ 9000 Mc/sec.

A closer inspection of the line shape at ~ 9000 Mc/sec revealed a marked asymmetry with the magnetic field pointing along the [111] direction. It was also found that the line width measured with H along the [110] direction gave a consistently higher value than with H along the [100] direction. These results suggested an anisotropic g value of the center which would result in an unresolved structure of the line. In order to test this hypothesis the experiments were repeated at 22700 Mc/sec[57] and a structure was indeed resolved. The results are shown in Fig. 17 and can be fitted by assuming an axially symmetric g tensor with the axis of symmetry pointing along the [111] directions. The two principal g-values are:

$$g_{[111]} = g_{\parallel} = 1.9978 \pm 0.0001$$

$$g_{\perp} = 1.9992 \pm 0.0001.$$

[52] E. Abrahams (private communication).

[53] Combrisson, Honig, and Townes, Compt. rend. 242, 2451 (1958).

[54] C. S. Fuller and J. A. Ditzenberger, Phys. Rev. 91, 193 (1953).

[55] I am indebted to C. S. Fuller for preparing all the Li-doped and heat-treated samples used in this work.

[56] A. Honig and A. F. Kip, Phys. Rev. 95, 1686 (1954).

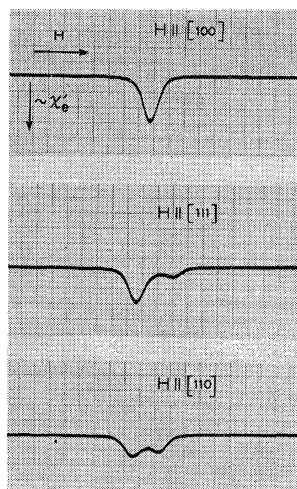[57] I am indebted to J. P. Gordon for the use of his K-band equipment and his assistance in this experiment.

Fig. 18. The ENDOR signal from Li-doped silicon ($\sim 3 \times 10^{16}$ Li/cm^3, $T = 1.25°$K, $\nu_e \simeq 9000$ Mc/sec). The additional structure on the Li^7 lines is due to a quadrupole interaction.

Because of the four equivalent [111] directions the expected ratio of the amplitudes of the resolved lines is 3–1 in the [111] direction and 1:1 in the [110] direction. The small deviation of this ratio in the [110] direction (see Fig. 17) is presumably due to a slight misalignment of the sample.

The line width (see Sec. IID) of the resonance line measured in the [100] direction was found to be

$$\Delta H = 2.3 \pm 0.1 \text{ oersteds.}$$

The relaxation time of the sample with 3×10^{16} Li/cm^3 was of the order of 10^{+2} seconds (see Part II).

The anisotropic g-value of Li indicates that the electronic wave function of this center, unlike that of the Group V donors, does not have tetrahedral symmetry. This is not too surprising in view of the fact that Li is an interstitial impurity, whereas the Group V donors from substitutional impurities. A possible position of the Li, consistent with the symmetry of the g tensor, would be along the [111] axis between the 000 and 333 position in the unit cell as indicated in Fig. 7.

The hf interaction of the electron with the Li^7 and Li^6 nuclei[7] was obtained by the ENDOR technique. Figure 18 shows part of the spectrum with the field pointing along the [111] direction. An additional structure is observed on the Li^7 lines (see arrows in Fig. 18). The separation of the two lines of this structure from the central peak is ± 37 kc/sec. In the other crystalline directions the pattern of this structure becomes more complicated and was not investigated in detail. In the sample doped with the enriched Li^6 isotope no corresponding structure was observed on the Li^6 lines. From this we conclude that the splitting of the Li^7 lines is due to an interaction between the electric field gradient and the quadrupole moment of Li^7 which is about one hundred times larger[39] than the quadrupole moment of Li^6. The hf interaction constants were obtained from the distance between the two central peaks with the
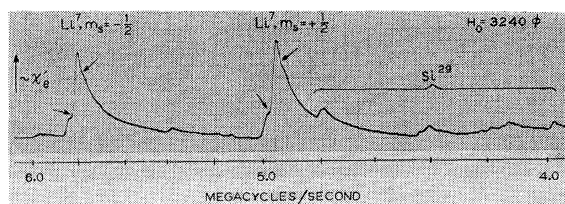
magnetic field pointing along the [111] directions. The values are

$$a(\text{Li}^7) = 0.845 \pm 0.003 \text{ Mc/sec,}$$
$$a(\text{Li}^6) = 0.316 \pm 0.001 \text{ Mc/sec;}$$

therefore,

$$|\Psi(0)|^2 = 0.33 \times 10^{22} \text{ cm}^{-3}.$$

The foregoing value is to be compared with $|\Psi(0)|^2 = 0.2 \times 10^{22}$ cm^{-3} obtained by Kohn and Luttinger[6] for an interstitial center with an ionization energy of 0.033 ev.

It is of interest to compare the experimentally determined ratio of the hf interactions

$$a(\text{Li}^7)/a(\text{Li}^6) = 2.67 \pm 0.01,$$

with the experimentally observed ratio of nuclear $g \sim$ values[58]

$$g(\text{Li}^7)/g(\text{Li}^6) = 2.6403 \pm 0.0008.$$

Since the hf structure anomaly for the Li^6-Li^7 pair[39] due a nuclear size effect is only about 1 part in 10^4, the larger observed discrepancy between the ratio of the a's and g's has to be attributed to a solid-state effect. Several such effects were discussed in connection with the Sb^{121}-Sb^{123} hf structure anomaly[59,17] and were found to be negligible. However, in the case of Li the effect due to the difference in zero-point vibration amplitudes for the two isotopes is more pronounced because of the smaller masses of the isotopes (i.e., larger amplitudes) and their larger fractional mass difference. The crude estimate of reference 17 when carried over to Li predicts a difference between the ratios of a and g of $\sim 1\%$ which is consistent with the experimentally observed value. An effect of presumably similar origin, was found by Klein[60] who observed a discrepancy of the ratio of the Knight shifts to the nuclear g values in the Li^{6,7} isotopes.

It should be pointed out again that we have taken the central peaks in order to determine the a's. Although

---

[58] This value was obtained from the ENDOR traces. It is more precise than the ratio of the hf interactions because the frequencies involved are higher. It is in agreement with the values obtained from nuclear resonance measurements (see reference 39, p. 173).

[59] I would like to thank R. G. Shulman for a stimulating discussion of these effects during which he pointed out the possible effect of lattice vibrations on the hf interaction.

[60] M. Klein (private communication).

this is a very plausible procedure, in view of the incomplete understanding of the structure of this line, it lacks at present rigorous justification.

In conclusion, we would like to mention an experiment performed on a silicon sample prepared by the floating zone method. As before 3×10^{16} Li/cm³ were diffused into the silicon. However, no electron spin resonance signal could be observed in this sample. One of the main differences between zone-refined and pulled crystals is the amount of oxygen present in the crystal. A pulled crystal has of the order of 10^{18} oxygens/cm³ [61] which suggests that perhaps a lithium-oxygen complex is required to produce a center that exhibits a paramagnetic resonance. Such complexes have been discussed by Pell.[62]

C. Heat Treatment Centers

It was shown by Fuller et al.[63] that when silicon is heated to temperatures between 300°C and 600°C donors are produced. The ionization energies of these centers varies between 0.033 ev and 0.13 ev[27] which indicates that one is not dealing with a unique center but with a variety of species. The recent work of Kaiser, Frisch, and Reiss[64] and Hrostowski and Kaiser[65] shows that the centers are due to different size aggregates of oxygens which in ordinary pulled crystals are dissolved in concentrations of the order of 10^{18} O/cm³.[61]

The observation of an electron spin resonance line due to this center has been reported by Fletcher and Feher.[66] The most striking feature of these centers is the lack of correlation between the total number of donors introduced by the heat treatment and the number of centers that give rise to a resonance signal. In the previous section a similar situation was discussed in connection with lithium diffused into zone refined silicon. The ratio of the total number of donors to the number of centers contributing to the resonance depends on the heat treatment (temperature and length of time) and varies from crystal to crystal. Variations in the g-value and line width were also observed between different samples. Since no systematic study of these variations was made, only a few representative results will be quoted.

One set of samples was cut from a crystal grown in a hydrogen atmosphere and was heat treated[55] for 24 hours at 430°C. The total number of donors introduced was $\sim 10^{16}$/cm³. About 30% of them contributed to the resonance signal. This number was obtained by comparing the integrated signal from this center with that obtained from a phosphorus doped silicon sample.

The inhomogeneously broadened line width was $2\Delta H = 1.5$ oersteds. The g value was 2.0023 ± 0.0001. The ENDOR spectrum did not show a resolved line. Only the broad line due to the weakly interacting Si²⁹ nuclei was observed [see Fig. 3(c)]. This again is consistent with having a variety of centers.

The second set of samples was obtained from a crystal grown in a helium atmosphere and heat treated in the same way as before. The total number of donors obtained during the heat treatment was again $\sim 10^{16}$/cm³. However, the number of centers contributing to the resonance signal was less than 10^{14}/cm³. In both crystals the number of electrically active impurities before the heat treatment was of the order of 10^{14}/cm³.

D. Iron

So far we have discussed only centers with ionization energies that are small in comparison to the energy gap. The electronic wave function of these "shallow" donors extends over hundreds of lattice points and can be described by the effective mass formulation of Kohn and Luttinger.[6] In addition several donors have been found which have deep levels (i.e., large ionization energies) associated with them. An example is Fe in silicon.[67] It has one donor level at 0.40 ev above the valence band and one 0.55 ev below the conduction band. The electron spin resonance from this center has also been reported by Ludwig et al.[68],‡

The samples used in our experiments were prepared by diffusing approximately 10^{16} Fe/cm³ into phosphorus doped silicon ($\sim 10^{16}$ P/cm³). The procedure has been described by Collins and Carlson[67] and should result in a center with the lower energy level. The experimental results on this sample are shown in Fig. 19. The resonance line exhibits a broad background and a narrow central peak that resolves further into a set of lines with a spacing of about 0.5 oersted. This spacing is independent of the applied magnetic field.[68] This would be consistent with assigning the origin of the splitting to the hf interaction of the electron with the Si²⁹ nuclei. The width of the broad background line varies with the direction of the magnetic field with respect to the crystalline axes. It was also found to depend on the method of preparation of the sample. The width $2\Delta H$ (in the [111] direction) varied in different samples between three and ten oersteds. This suggests that the width of the background line may be governed either by clumping effects or strains in the sample. From the spin-spin interactions discussed in Part II it seems clear, however, that the resonance is due to iron atoms

[61] Kaiser, Keck, and Lange, Phys. Rev. 101, 1264 (1956).

[62] E. M. Pell, presented at the Brussels Conference, 1958.

[63] Fuller, Ditzenberger, Hannay, and Buehler, Phys. Rev. 96, 833 (A) (1954).

[64] Kaiser, Frisch, and Reiss, Phys. Rev. 112, 1546 (1958).

[65] H. J. Hrostowski and R. H. Kaiser, Phys. Rev. Letters 1, 199 (1958).

[66] R. C. Fletcher and G. Feher, Bull. Am. Phys. Soc. Ser. II, 1, 125 (1956).

[67] C. B. Collins, Bull. Am. Phys. Soc. Ser. II, 1, 49 (1956); C. B. Collins and R. O. Carlson, Phys. Rev. 108, 1409 (1957).

[68] Ludwig, Woodbury, and Carlson, Phys. Rev. Lett. 1, 295 (1958).

‡ Note added in proof.—An additional resonance spectrum was reported in iron doped silicon by Ludwig et al. [Ludwig, Carlson, and Woodbury, Bull. Am. Phys. Soc. Ser. II, 4, 22 (1959)]. This additional spectrum was subsequently attributed by them to Chromium impurities.
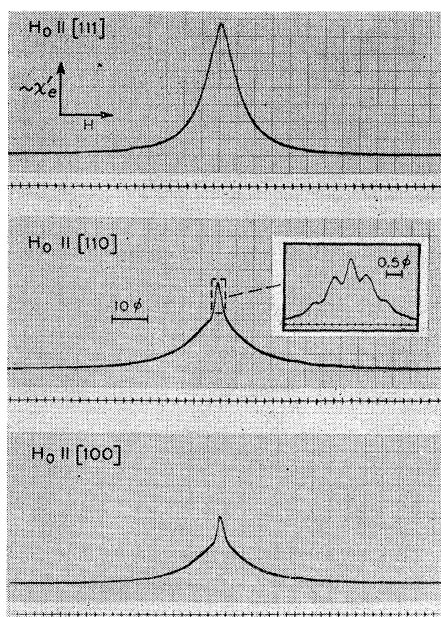
FIG. 19. Electron spin resonance signal from iron doped n-type silicon ($\sim 10^{16}$ Fe/cm^3, $\sim 10^{16}$ P/cm^3, $T = 1.25°$K, $\nu_e \simeq 9000$ Mc/sec). Note the difference in line shape as the magnetic field points along the different crystalline axes. By decreasing the sweep speed, the center of the line was resolved into several components.

that are reasonably well dispersed throughout the silicon. The electronic g-value of the center at 1.25°K was found to be $g = 2.0702 \pm 0.0001$.

Heating the sample for 24 hours at 85°C produced no noticeable change in the resonance signal. This is surprising in view of the reported change in the energy levels of this center during such a heat treatment. The resonance signal disappears when the sample is heated to 250°C for one hour.

The nature of this spectrum bears no resemblance to the Fe^{+++} and Fe^{++} spectra observed in ionic crystals[69] and is at present not understood.

Other deep centers in silicon in which electron spin resonances were observed include Mn impurities studied by Ludwig et al.[70] and centers associated with radiation damage studied by Schultz-Du Bois et al.[71] and Bemski et al.[72]

E. Centers Associated with the Surface

In the early resonance experiments on silicon an additional resonance line was observed[4,73] and was

thought to be associated in some way with the surface of the silicon. This conclusion is consistent with our observations.

We have found that a resonance line appears when the surface of the sample is sandblasted, polished or when the crystal is broken up into small particles. The line could not be eliminated by treating the samples for a few minutes with concentrated HCl, HNO$_3$, or HF. None of these acids remove an appreciable amount of silicon but change the surface conditions of the samples (i.e., produce or remove oxide films). If, however, $\sim 10^{-4}$ cm of the silicon surface is removed by a HF+HNO$_3$ etch, the resonance line disappears. If such a sample is sandblasted or polished the resonance line reappears. This cycle of etching and sandblasting was repeated and found to be reproducible. This behavior suggests that the paramagnetic centers are associated with the damage created during the mechanical treatment of the samples and may extend through many atomic layers.

The total number of centers was estimated by comparing the integrated resonance signal of these centers with the signal obtained from a known amount of copper sulphate. When the silicon samples were sandblasted with 600 mesh of SiC, $\sim 3 \times 10^{14}$ centers/cm^2 were created. The resonance line was homogeneously broadened ($T = 1.25°$K, $\nu_e = 9000$ Mc/sec) with a relaxation time of $\sim 10^{-5}$ sec and a line width of 6 oersteds (full width between inflection points of the resonance line which in this case is proportioned to $d\chi''/dH$). The electronic g-value was 2.0061 $\pm$ 0.0002.

The same resonance line was observed both in n-type ($\sim 2 \times 10^{14}$ P/cm^3) and p-type ($\sim 5 \times 10^{14}$ B/cm^3) silicon. We believe that the resonance line previously attributed[74] to free holes within the bulk of silicon is the same as the "surface resonance" described here.

F. Effect of Germanium on the Phosphorus Centers in Silicon

Silicon and germanium form substitutional alloys in which the atoms are situated randomly at the lattice sites of a diamond-type crystal. The band structure of such an alloy has been discussed by Herman.[75] The
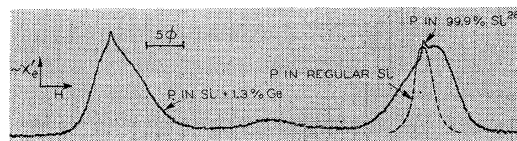

FIG. 20. Electron spin resonance signal from phosphorus-doped silicon with 1.3 atomic percent of germanium. ($T = 1.25°$K, $\nu_e \simeq 9000$ Mc/sec). The broadening of the line is due to variations in the value of $|\Psi(0)|^2$. The two markers on the trace were obtained from a separate phosphorus-doped silicon sample with isotopically purified Si^{28}.

[69] See for instance the review article by K. D. Bowers and J. Owen, in Reports on Progress in Physics (The Physical Society, London, 1955), Vol. 18, p. 304.

[70] Ludwig, Woodbury, and Carlson, International Conference on Semiconductors, Rochester, New York, 1958, published in J. Phys. Chem. Solids 8, 490 (1959).

[71] Schultz-Du Bois, Nisenoff, Fan, and Lark-Horowitz, Phys. Rev. 98, 1561 (1955).

[72] Bemski, Feher, and Gere, Bull. Am. Phys. Soc. Ser. II, 3, 135 (1958).

[73] Portis, Kip, Kittel, and Brattain (private communication).

[74] F. K. Willenbrock and N. Blombergen, Phys. Rev. 91, 1281 (1953).

[75] F. Herman, Phys. Rev. 95, 847 (1954).

effect on the spin resonance behavior of phosphorous-doped silicon (3×10^{16} P/cm^3) was investigated with 1.3% of the silicon atoms replaced by germanium. The results are illustrated in Fig. 20 and may be summarized as follows:

(1) The line shape is asymmetric and the width increased by a factor of two over the width in a pure silicon crystal. This increase in width is due to a variation of the hf interaction from one donor to another. This was proven by repeating the experiment on an alloy with only 0.4% of germanium. In this case the widths of the ENDOR lines due to the phosphorus and Si^{29} nuclei were larger by a factor of ~20 than the corresponding widths in a pure Si crystal.

(2) From the line shape one finds that the change in $|\Psi(0)|^2$ may be either positive or negative. It should be noted that effects like variations in the dielectric constant would result only in a decrease in $|\Psi(0)|^2$. The average hf interaction as measured from the distance between the centers of gravity of the two lines is reduced from 117.5 Mc/sec (see Sec. II-C-4) to 113.4 Mc/sec. The distance between the peaks of the lines is 121.5 Mc/sec. The spread in the wave function as obtained from the total line width is about 16 Mc/sec, as compared with ~0.05 Mc/sec in a pure silicon sample.

(3) The g-value of the phosphorus donor electron in the 1.3% alloy is lower than in the pure silicon crystal by an amount

$$\delta g = g_{\text{Ge-Si}}(P) - g_{\text{Si}}(P) = (-5.6\pm0.1)\times10^{-4}.$$

Since a Ge-Si alloy is not a periodic structure, the crystal parameters (e.g., effective mass, bandgap, $k_0/k_{\max}$, etc.) do not have sharp values. One might, therefore, expect local variations in $|\Psi(0)|^2$ which would result in an increased line width. The additional g-shift is presumably due[25] to the larger spin-orbit coupling in germanium. So far, no calculations have been made to account for these effects in a quantitative way.

IV. ACKNOWLEDGMENTS

I profited from discussions with many members of the Bell Telephone Laboratories, but I am especially indebted to P. W. Anderson and W. Kohn for the many helpful and stimulating discussions, suggestions and criticism and in particular for their cooperation in the identification of the ENDOR lines. I had also many valuable conversations with E. Abrahams, J. A. Burton, and J. Eisinger. I would like to thank E. A. Gere for his expert assistance in carrying out the experiments, J. P. Gordon for the experiments performed on his 23 kMc/sec equipment, R. C. Fletcher for his collaboration in the early stages of this work, D. Shechter and B. Mozer for calculating the data of Fig. 7, C. S. Fuller for supplying us with the Li-doped and heat treated samples, G. Bemski and R. O. Carlson for
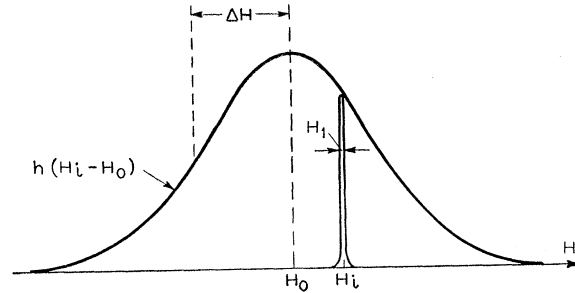

FIG. 21. Distribution of spin packets in an inhomogeneously broadened line.

carrying out the Fe diffusion, as well as the crystal growing group of the Bell Telephone Laboratories for supplying us with the numerous samples used in this work. I would like to thank Miss C. L. Monahan for computational help.

VI. APPENDIX

(A) Behavior of an Inhomogeneously Broadened Line Under Adiabatic Fast Passage Conditions

(1) Line Shape in the Absence of Magnetic Field Modulation

An inhomogeneously broadened[13] line arises from a distribution of spins resonating at different magnetic fields H_i centered about H_0 (see Fig. 21). Following Portis's treatment[13,41] the distribution is given by the shape function $h(H_i-H_0)$ subject to the normalizing condition

$$\int_{-\infty}^{+\infty} h(H_i-H_0)dH_i=1. \qquad (19)$$

The magnetization due to spins having resonant fields in an interval dH_i is given by

$$dM_i = M_0 h(H_i-H_0)dH_i, \qquad (20)$$

where M_0 is the static magnetization which may also be written as $\chi_0 H$. Under adiabatic fast passage conditions[10] one is interested only in the part of the magnetization that is in phase with the microwave field H_1 (i.e., χ'). Going into a frame of reference[76] rotating with the microwave frequency $\omega=\gamma H_i$, one obtains for the projection of the magnetization along H_1 (see Fig. 22)

$$dM_{ix}=dM_i \cos\theta_i=\pm dM_i\frac{H_1}{[H_1^2+(H_i-H)^2]^{\frac{1}{2}}}, \qquad (21)$$

where H_1 is the amplitude of the circularly polarized component of the microwave field. The plus sign corresponds to the establishment of equilibrium of the magnetization above the resonance field, i.e., $(H-H_0)>0$ and the minus sign below the resonance field.

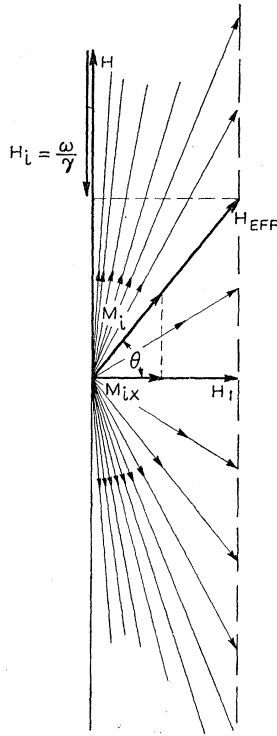[76] Rabi, Ramsey, and Schwinger, Revs. Modern Phys. 26, 167 (1954).

FIG. 22. The effective magnetic field seen by different spin packets in the rotating coordinate system. Experimentally one observes the magnetization along the microwave field H_1 [see Eqs. (22), (24)].

Assuming that the relaxation times are longer than $1/\gamma H_1$ the line width of an individual spin packet will be given by H_1. For the contribution of all the spin packets to the magnetization along H_1, one obtains

$$M_x(H) = \pm M_0 \int_{-\infty}^{+\infty} \frac{h(H_i - H_0)}{[1 + (H_i - H)^2/H_1^2]^{\frac{1}{2}}} dH_i. \quad (22)$$

This expression represents the general relation between the observed line shape $M_x(H)$ and the distribution of spin packets given by the shape function $h(H_i - H_0)$. In order to evaluate Eq. (22) let us assume that the shape function is a Gaussian, i.e.,

$$h(H_i - H_0) = \frac{1}{\Delta H}\left(\frac{0.69}{\pi}\right)^{\frac{1}{2}} \exp\left[-\left(\frac{H_i - H_0}{\Delta H}\right)^2 0.69\right], \quad (23)$$

where ΔH is the half-width of the distribution at the half power point.

From Eqs. (22) and (23) one gets for the observed line shape

$$M_x(H) = \pm \frac{M_0}{\Delta H}\left(\frac{0.69}{\pi}\right)^{\frac{1}{2}}$$

$$\times \int_{-\infty}^{+\infty} \frac{\exp\{[-(H_i - H_0)^2/(\Delta H)]0.69\}}{[1 + (H_i - H)^2/H_1^2]^{\frac{1}{2}}} dH_i. \quad (24)$$

An inspection of the above expression shows that for vanishingly small H_1 the Gaussian envelope remains undistorted.

For larger H_1, the above integral can be evaluated by an appropriate expansion, and one obtains

$$M_x(H) = \pm M_0 \left(\frac{0.69}{\pi}\right)^{\frac{1}{2}} \frac{H_1}{\Delta H} \exp(-0.69x^2)e^{\beta}K_0(\beta)$$

$$\pm 1.38\beta x^2[K_1(\beta) - K_0(\beta)]$$

$$\pm \tfrac{1}{3}(1.38\beta)^2 x^4[K_0(\beta) - (1 - \tfrac{1}{2}\beta^{-1})K_1(\beta)], \quad (25)$$

where $x = (H - H_0)/\Delta H$, $\beta = 0.69H_1^2/(2\Delta H^2)$ and K_0, K_1 are the Bessel functions of zeroth and first order.[77]

Assuming that $\beta \ll 1$ and $x\beta^{\frac{1}{2}} < 1$, expression (25) simplifies to

$$M_x(H) = \pm M_0 \left(\frac{0.69}{\pi}\right)^{\frac{1}{2}} \frac{H_1}{\Delta H} \exp(-0.69x^2)e^{\beta}K_0(\beta)$$

$$\pm 1.38\beta x^2\left(1 + \frac{0.69}{3}x^2\right)K_1(\beta). \quad (26)$$

Equation (26) is plotted in Fig. 23 for different values of $\Delta H/H_1$. In our experiments $\Delta H/H_1$ was chosen to be approximately 10^3 which makes the observed line width about 8% larger than would correspond to e Gaussian distribution of spin packets. The ratio of tha observed line width to the width of the distribution of spin packets for different values of $\Delta H/H_1$ is plotted in Fig. 24.

The plot of Fig. 23 shows all the curves normalized to the maximum magnetization. One can get the value of the magnetization for $x = 0$ from Eq. (26) by expanding K_0 for small arguments[77]

$$M_x(H_0) \simeq \pm \frac{\chi_0 H}{\Delta H}\left(\frac{0.69}{\pi}\right)^{\frac{1}{2}} H_1 \ln\left(\frac{1.7\Delta H}{H_1}\right). \quad (27)$$

The susceptibility $\chi' = M_x/2H_1$ is then given by

$$\chi'(H_0) \simeq \pm \frac{\chi_0}{2} \frac{H}{\Delta H}\left(\frac{0.69}{\pi}\right)^{\frac{1}{2}} \ln\left(\frac{1.7\Delta H}{H_1}\right). \quad (28)$$
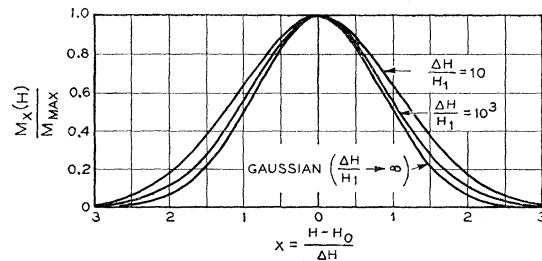

FIG. 23. The line shape of an inhomogeneously broadened line observed under adiabatic fast passage conditions for various ratios of $\Delta H/H_1$. The distribution of spin packets is assumed to be Gaussian.

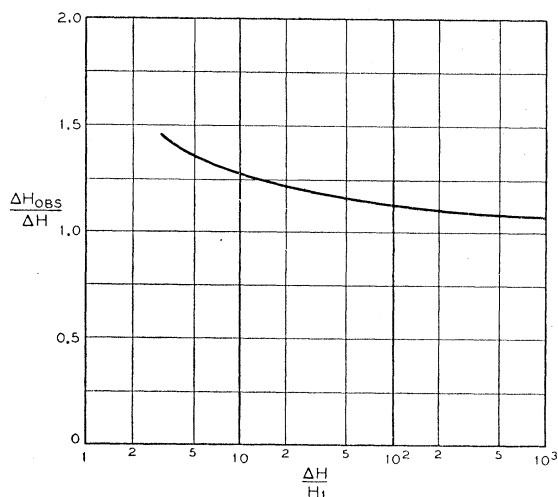[77] E. T. Shittaker and G. N. Watson, Modern Analysis (Cambridge University Press, Cambridge, 1950), p. 375.

FIG. 24. ratio of the observed width to the width of the distribution of spin packets for different values of $\Delta H/H_1$.

The above expression agrees with the one given by Portis.[43]

From Eq. (28) one sees that, neglecting the logarithmic term, $M_x(H_0)$ is proportional to H_1. This behavior can be qualitatively understood from Fig. 22. For a *single* spin packet the maximum magnetization M_x is independent of H_1 and equal to M_i for $\theta = 0$. This is the same as one obtains for a homogeneously broadened line under adiabatic fast passage conditions. However, if we are dealing with an inhomogeneously broadened line, the angle θ that each spin packet makes with H_1 decreases as H_1 increases and therefore it contributes more effectively to M_x.

(2) Line Shape with Magnetic Field Modulation

In this section we wish to consider the amplitude of the signal when the magnetic field is set to the center of the resonance line and is modulated over a fraction of the line width thereby flipping back and forth all the spin packets that are within the modulation amplitude. This corresponds to the experimental situation encountered in the ENDOR technique and with an additional linear variation of the magnetic field describes the situation that is commonly encountered in ordinary paramagnetic resonance techniques. The spin packets will be affected differently according to how far they are removed from the value of the dc magnetic field H_0. Figure 25 illustrates this situation for one particular spin packet which has an amplitude M_i before the modulation field is turned on. The problem is to find the steady-state value M_F to which M_i decays after many modulation cycles and the time constant associated with this process.

We assume again that the spin packets are traversed under idealized adiabatic fast passage conditions. This process should therefore not destroy the magnetization during a single passage but merely turn it over so that

during the time t_1 (see Fig. 25) the magnetization will point opposite to the magnetic field. In this position the magnetization will decay to its equilibrium value with its characteristic spin lattice relaxation time T. The magnetization after a different number of traversals $(N-1)$, N, $(N+1)$ as indicated in Fig. 25 is then given by

$$M_N = M_{N-1}e^{-t_1/T} - M_i(1 - e^{-t_1/T}), \quad (29)$$

$$M_{N+1} = M_N e^{-t_2/T} + M_i(1 - e^{-t_2/T}), \quad (30)$$

where t_2 is the time interval per cycle during which M points along H. After a number of passages a steady-state is reached in which case $M_{N-1} = M_{N+1}$ and one obtains

$$M_N' = M_i \frac{2e^{-t_1/T} - e^{-(t_1+t_2)/T} - 1}{1 - e^{-(t_1+t_2)/T}}, \quad (31)$$

$$M_{N+1}' = M_i \frac{2e^{-t_2/T} - e^{-(t_1+t_2)/T} - 1}{1 - e^{-(t_1+t_2)/T}}, \quad (32)$$

where M_N' is the observed steady-state value of the magnetization after the time interval t_1 and M_{N+1} after the time interval t_2. (See Fig. 25.) Equations (31) and (32) are identical with the equations used by Chiarotti et al.[78] to measure nuclear relaxation times.

In all the experimental cases that we studied $t_1 \ll T$ and $t_2 \ll T$ which simplifies the expression to

$$M_N' = M_{N+1}' = M_i(t_2 - t_1)/(t_1 + t_2) = M_F. \quad (33)$$

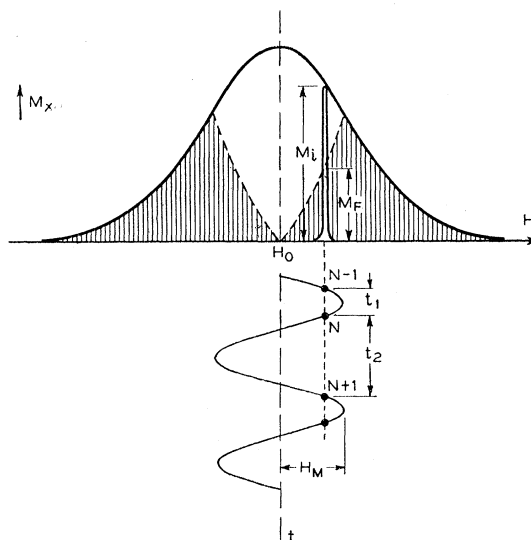For a sinusoidal field modulation $H = H_0 + H_M \sin\omega_m t$

FIG. 25. The idealized behavior of an inhomogeneously broadened line when a sinusoidal field modulation is applied. The initial magnetization M_i decays to the steady-state magnetization M_F. The spin packets are traversed under adiabatic fast passage conditions.

[78] Chiarotti, Christiani, Giulotto, and Lanzi, Nuovo cimento 12, 519 (1954).

it follows from (33) that the magnetization M_F will be given by

$$M_F = M_i(2/\pi) \sin^{-1}(H-H_0/H_M). \qquad (34)$$

This steady-state magnetization is indicated by the dotted line in Fig. 25.[79]

In order to evaluate the output signal one needs to know the time variation of M_F. From Eq. (34) we see that M_F will vary linearly with time, i.e., one gets a triangular output. Since the signal is fed into a narrow band amplifier we are only interested in the fundamental frequency component which is

$$\text{steady-state output signal} \propto M_i(8/\pi^2) \cos\omega_M t, \qquad (35)$$

where ω_M is the modulation frequency.

Before the steady-state condition as given by Eq. (35) is reached the output signal will be larger since the magnetization did not have a chance to decay to its final value. This means that if one turns on the microwave power, M_i will at first be a constant resulting in a square wave output whose fundamental will be given by

$$\text{transient output signal} \propto M_i(4/\pi) \cos\omega_M t. \qquad (36)$$

Thus the expected steady-state output signal should be smaller by $(2/\pi)$ than the signal obtained at $t=0$.

The foregoing considerations lead immediately to the simple "passage cases" which were the ones most commonly dealt with in the semiconductor work described in this article.

If the modulation field satisfies the adiabatic fast passage condition $(\omega_M H_M \ll \gamma H_1^2; \omega_M \gg 1/T)$ and the modulation amplitude is large in comparison to the spin packet $(H_M \gg H_1)$ and one traverses the resonance line in a time short compared to the spin lattice relaxation time, the output of the narrow band amplifier will be obtained by combining Eqs. (36) and (24).

$$\text{Signal} \sim \left(\frac{9}{\pi}\right) M_0 \int_{-\infty}^{+\infty} \frac{M(H_i-H_0)}{[1+(H_i-H)^2/H_1^2]^{\frac{3}{2}}}$$
$$\times (\cos\omega_M t) dH_i, \qquad (37)$$

or for small enough H_1 the susceptibility $\chi'(H)$ will be given by:

$$\chi'(H) = \frac{2\chi_0}{\pi}\frac{H}{\Delta H}\left(\frac{0.69}{\pi}\right)^{\frac{1}{2}} \exp\left[-\left(\frac{H_i-H_0}{\Delta H}\right)^2\right]0.69$$
$$\times (\cos\omega_M t) \ln\left(\frac{1.7\Delta H}{H_1}\right). \qquad (38)$$

If one traverses the line in a time long in comparison to a relaxation time, the signal will be of the same

form as Eq. (38) but with an amplitude reduced by $2/\pi$. It is interesting to note that the output signal is independent of the amplitude of the field modulation. This, of course, holds only as long as our assumption $H_M > H_1$ is satisfied. This behavior was experimentally verified by observing the output signal as a function of H_M. The amplitude of the signal remained approximately constant for $H_M > H_1$ and started to decrease as H_M approached the value of H_1. This procedure could therefore be used to determine the width of spin packets in inhomogeneously broadened lines.

The ac signal given by Eq. (38) is usually converted to a dc signal by means of a phase sensitive detector.[22] In this case, as opposed to the direct detection scheme discussed previously, the sign of the signal is independent of the value of the external magnetic field at which the magnetization is equilibrated. Other passage cases have been treated by Portis.[40,41]

(3) Rate of Saturation of an Inhomogeneously Broadened Line

We next inquire what happens when the magnetic field is set to $H_0+H_M \cos\omega_M t$ and the microwave power is turned on in a time much shorter than the relaxation time T. This is closely related to what happens in an ENDOR experiment where instead of the microwaves power being turned on, the population difference is suddenly changed. In both cases we are concerned with the rate at which the signal is being saturated, i.e., the decay of the signal from the value given by Eq. (36) to that given by Eq. (35). This effect is responsible for the trailing off of the ENDOR signal as seen in Figs. 3(a), (4), and (13). It is characteristic of the transient mode of operation associated with the long relaxation times encountered in silicon. In systems with a shorter relaxation time a steady-state mode of operation is possible.[80]

From Eqs. (29) and (30) one obtains

$$M_{N+1} = M_i(1-2e^{-t_2/T}+e^{-(t_1+t_2)/T})$$
$$+M_{N-1}e^{(t_1+t_2)/T}. \qquad (39)$$

After m modulation cycles the amplitude M_m will then be given by

$$M_m = M_i(1-2e^{-t_2/T}+e^{-\alpha})(1+e^{-\alpha}+e^{-2\alpha}+\cdots e^{-m\alpha})$$
$$+M_i e^{-(m+1)\alpha}$$
$$= M_i(1-2e^{-t_2/T}+e^{-\alpha})\frac{e^{-(m+1)\alpha}-1}{e^{-\alpha}-1}+M_i e^{-(m+1)\alpha}, \qquad (40)$$

where $\alpha = (t_1+t_2)/T$. For $m\alpha \ll 1$, this expression can be

---

[79] Note that in Fig. 25, the modulation amplitude has been exaggerated. In practice it is much smaller than the line width so that we can neglect the variation of M_i over the modulation field.

[80] Such systems include for instance color centers in alkali halides. A brief discussion of the requirements of this mode of operation was given by G. Feher, *Proceedings of the Kamerlingh-Onnes Memorial Conference on Low-Temperature Physics, Leiden, 1958* [Suppl. Physica 24, 80 (1958)].

expanded to give

$$M_m \simeq M_i [1 - 2(m+1)t_1/T].\qquad(41)$$

The number of modulation cycles in a time t is $t/(t_1+t_2)$. The initial decay of the magnetization is then described by

$$M(t) \simeq M_i \left[1 - 2\left(\frac{t_1}{t_1+t_2}\right)\frac{t}{T}\right],\qquad(42)$$

where $t_1/(t_1+t_2)$ is the fraction of the modulation cycle during which the magnetization points opposite to the magnetic field. This means that the rate at which the spin packets saturate is smallest for the ones near the extreme excursions of the field modulation. The spin packet at H_0 (i.e., $t_1=t_2$) decays fastest with an initial time constant equal to the relaxation time T.

(4) Comparison of the Predicted Behavior with Experiment

In all the preceding sections we have assumed the absence of spin-spin interactions. The predictions based on this assumption are in general qualitative agreement with the experimental findings (e.g., one observes the line shape as given by Fig. 23; one can "burn holes" in the lines, etc.). However, in some cases serious quantitative discrepancies are observed. All of them can be traced to one phenomenon, namely, the partial destruction of the magnetization when the resonance line (or a part of it) is traversed. The origin of this effect lies presumably in the spin diffusion process as described in Part II of this paper but more generally it could be due to any interaction that causes a "dephasing" of the spin packets.

The most clear-cut experiment that demonstrates the loss of magnetization is illustrated in Fig. 26, which shows several successive traversals of the resonance line. This is accomplished by sweeping the magnetic field from a value below to a value above the resonance field H_0 and then reversing it. No other field modulation was applied in this experiment. The trace in Fig. 26 was derived directly from the output of the i.f. amplifier. Since the time between two successive traversals ($t=10$ seconds) was short in comparison to the relaxation time ($T_s=30$ minutes), one would have expected the magnetization to remain unchanged. That this is not the case is clearly illustrated in Fig. 26, where a fractional loss of the magnetization of ~ 10–20% is observed after each passage. This effect, incidentally, should be taken into account in the polarization of nuclei by the method of adiabatic fast passages[81] and plays also an important part in the operation of two level solid-state masers.[44,53]

There are several other consequences of this effect: (1) When a field modulation detection scheme is used (see Sec. II D-3) the loss of magnetization is much more

---

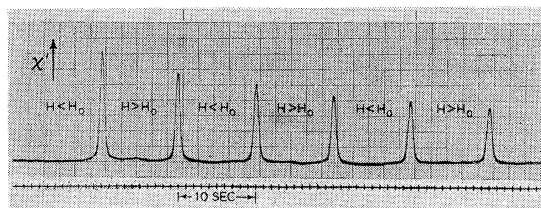[81] G. Feher, Phys. Rev. **103**, 500 (1956).

FIG. 26. Reduction of the magnetization during successive adiabatic fast passages. The time between two passages is short in comparison to the electron spin relaxation time T_s ($T_s \simeq 40$ minutes). No magnetic field modulation was used to observe the signal. The sample is phosphorus-doped silicon ($\sim 10^{16}$ P/cm^3, $T=1.25°$K, $\nu_e \simeq 9000$ Mc/sec).

pronounced resulting under certain conditions in a complete saturation of the line. This is because the magnetic field sweeps many times over a given set of spin packets, *each* time causing a reduction in the magnetization. This was found to be a convenient property in the study of relaxation times (see Part II). The magnetization is destroyed by sweeping through the line with the field modulation turned on. The growth of the magnetization is subsequently observed by sweeping through the line after different time intervals. (2) The rate of saturation of the line is faster than predicted by Eq. (42) and the steady-state amplitude of the signal is smaller than given by Eq. (35). This makes it difficult to derive quantitatively the absolute magnitudes of the ENDOR signals. (3) The shape of the region that has been saturated by applying a sinusoidal field modulation over a fraction of the line differs from the one shown in Fig. 25. The saturation is more complete than predicted at the extreme excursions of the field modulation sweep (see Fig. 2). This presumably is because the time spent at those extreme spin packets is longer than at the others.

One could rework Eqs. (29) and (30) in a purely phenomenological way by assuming a given loss of magnetization per passage. However, at present such a treatment would be only of limited use since the detailed dependence of the loss of the magnetization on the microwave power and the time spent on the line is not understood.

(B) Relative ENDOR Amplitudes

As pointed out in Sec. C-2e the relative amplitudes of the ENDOR lines serve as an additional tool in the identification of the lines. In this section the problem is considered under the following simplifying conditions: (1) All spin packets that give rise to the ENDOR lines are turned over and saturated by the same amount. (2) The line width of all the individual lines is the same. It will be shown that even under these simplifying assumptions the relative amplitudes will not be equal to the relative number of occupied lattice sites but will depend on the hf interaction a_l and the value of the DC magnetic field with respect to the center of the electron spin resonance line.
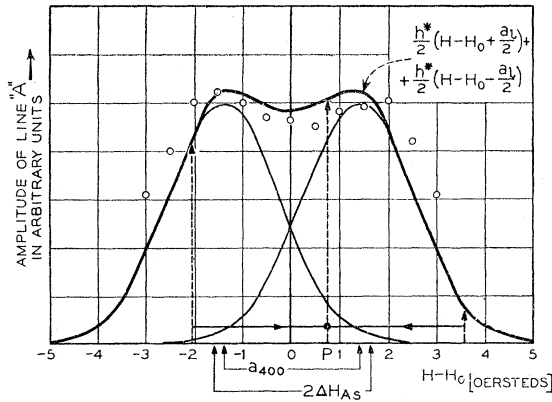
FIG. 27. ENDOR amplitude of line A (see Sec. II C-2) in arsenic-doped silicon for different settings of the magnetic field with respect to the center of the line. Solid curve indicates expected amplitude, circles represent experimental points. Arrows pointing towards P indicate the contribution to the magnetization from two sets of spin packets. ($\sim 2 \times 10^{16}$ As/cm^3, $T = 1.25°$K, $\nu_e \simeq 9000$ Mc/sec.)

Let us suppose that the electron resonance line at the microwave frequency ν_e and the corresponding external magnetic field H is saturated. If one now flips a Si^{29} nucleus at the lth lattice site which has a hf interaction a_l, the observed ENDOR signal will be caused by spin packets that see an effective field $H \pm a_l$ and upon application of the proper frequency cause a partial desaturation of the microwave line at H. (The $\pm$ sign arises from the fact that the Si^{29} moment can be either parallel or antiparallel to the direction of the electron spin.) The amplitude of the signal (i.e., the amount of desaturation) will then be proportional to the number of Si^{29} nuclei at the lth lattice site which see an effective field $H \pm a_l$.

The distribution of resonant fields of centers having a single[82] lth lattice site occupied by a Si^{29} nucleus may

[82] For simplicity we will not consider centers having two or more lattice sites occupied with Si^{29} nuclei. In view of the small fractional abundance of Si^{29} (0.047) this is quite a good approximation.

be obtained as follows. One imagines that all the Si^{29} nuclei are removed from the lth lattice site, and then the normalized shape function due to the hf interaction of all (except the lth Si^{29}'s will be given by $h^*(H-H_0)$. This shape function is the same as the one defined in Appendix A-1 modified in order to take into account the removal of the Si^{29} from the lth lattice site. The reintroduction of the Si^{29} will shift the distribution by $\pm \frac{1}{2} a_l$ and one obtains for the distribution of Si^{29} spins pointing along the field $\frac{1}{2} h^*(H-H_0-\frac{1}{2} a_l)$ and against the field $\frac{1}{2} h^*(H-H_0+\frac{1}{2} a_l)$. If one sets the magnetic field to a given value H, spin packets may be flipped from both distributions. The amplitude A of the ENDOR signal will then be proportional to

$$A_l \sim n_l[\tfrac{1}{2} h^*(H-H_0+\tfrac{1}{2} a_l) + \tfrac{1}{2} h^*(H-H_0-\tfrac{1}{2} a_l)], \quad (43)$$

where n_l is the number of equivalent Si lattice points of the lth site. Setting the magnetic field at the center of the electron resonance line $(H=H_0)$ the relative amplitudes of the ENDOR lines will be given by

$$A_l(0) = n_l h^*(\tfrac{1}{2} a_l). \quad (44)$$

Figure 27 illustrates the above discussion for line A (see Sec. II C-2) in As-doped silicon. The distribution h^* was assumed to be Gaussian with an effective full width $\Delta H_{\rm rms}^*$ given by

$$\Delta H_{\rm rms}^{*2} = \Delta H_{\rm rms}^2 - n_l f a_l^2, \quad (45)$$

where $\Delta H_{\rm rms}$ is the experimentally observed line width corrected for passage effects. (See Appendix A-1.) The dotted arrows indicate the spin packets that contribute to the ENDOR signal when the magnetic field is set to P. The circles on the graph represent experimental points normalized to fit the predicted curve. Although the agreement between the experimental values and the theory is not perfect, the essential features of this simple treatment seem to be borne out.
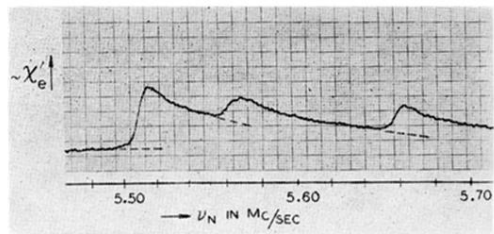
FIG. 13. Expanded trace of line B in As-doped silicon (see Fig. 4) with the magnetic field along the $[111]$ direction. The dotted lines represent the base lines from which the relative amplitudes are measured. Note from Fig. 10 that the expected ratio of amplitudes is 2:1:1 in approximate accord with the above trace. (8×10^{16} As/cm³, $T = 1.25°$K, $H_0 \simeq 3050$ oersteds.)
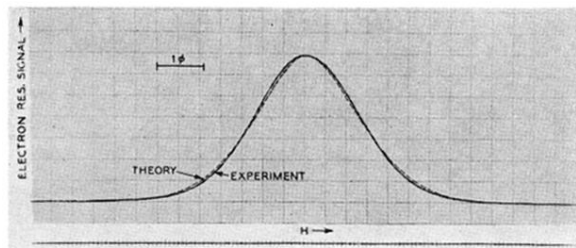
FIG. 14. Electron spin resonance line shape in phosphorus-doped silicon (1.5×10^{16} P/cm³, $T = 1.25°$K, $H_0 \simeq 3200$ oersteds). Magnetic field modulation was used and the microwave bridge was sensitive to the dispersion mode. The dotted line represents the expected shape as discussed in Appendix A-2.

FIG. 15. Electron spin resonance signals from two silicon samples. The central line is due to conduction electrons in a heavily doped sample $(3 \times 10^{18}$ P/cm³). The sample with $\sim 5 \times 10^{15}$ As/cm³ and $\sim 5 \times 10^{15}$ P/cm³ exhibits hf structure due to localized electrons. Field markers are derived from a proton sample. Note the difference in line shapes characteristic of "slow" and "adiabatic fast" passages.[10] (See Appendix A.) $(T = 1.25°K,$ $\nu_e = 8845.3$ Mc/sec.)

Fig. 16. Electron spin resonance signal from silicon doped with varying amounts of phosphorus. The range covers the transition from localized centers (a) to free carriers (d) as were used for the g-marker. For concentrations between these two extrema the observed resonance signal is due to clusters of phosphorus atoms[15] (b,c). This region marks the beginning of the impurity band conduction process. The different line shapes are a result of the change in relaxation times which cause the transition from "adiabatic fast" to "slow" passage conditions[10] (see Appendix A) ($T = 1.25°K$, $\nu_e \simeq 9000$ Mc/sec).
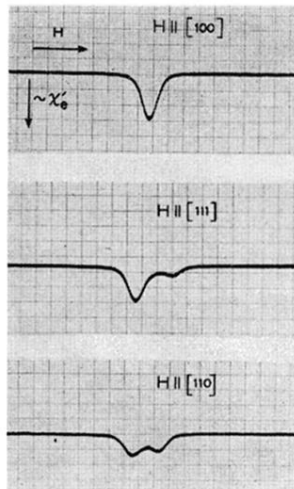
Fig. 17. Electron spin resonance signal from Li-doped silicon with the magnetic field pointing along the different crystalline directions ($\sim 3 \times 10^{16}$ Li/cm^3, $T = 1.25°$K, $\nu_e \simeq 22700$ Mc/sec). The splitting is due to an anisotropic g-value. This indicates that the wave function of the donor electron does not have tetrahedral symmetry.
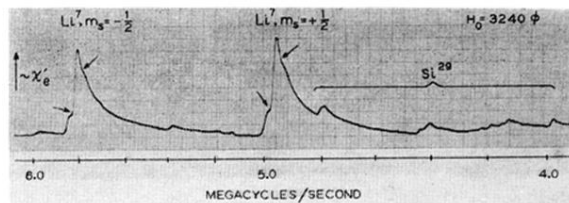
FIG. 18. The ENDOR signal from Li-doped silicon ($\sim 3 \times 10^{16}$ Li/cm³, $T = 1.25°$K, $\nu_e \simeq 9000$ Mc/sec). The additional structure on the Li⁷ lines is due to a quadrupole interaction.
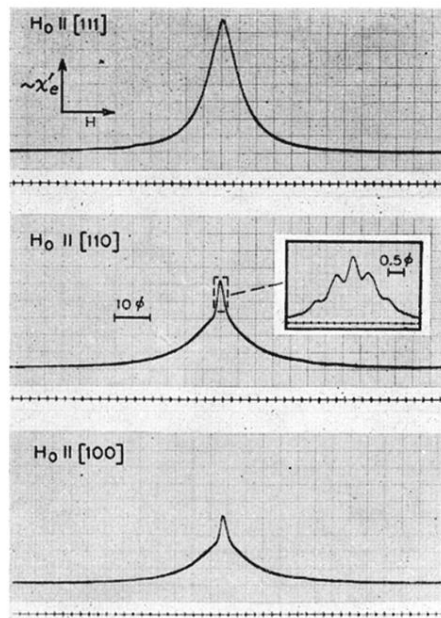
FIG. 19. Electron spin resonance signal from iron doped *n*-type silicon ($\sim 10^{16}$ Fe/cm^3, $\sim 10^{16}$ P/cm^3, $T = 1.25°$K, $\nu_e \simeq 9000$ Mc/sec). Note the difference in line shape as the magnetic field points along the different crystalline axes. By decreasing the sweep speed, the center of the line was resolved into several components.
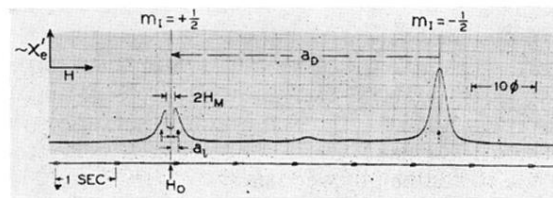
FIG. 2. Demonstration of the inhomogeneous broadening of the donor resonance in phosphorus-doped silicon (5×10^{16} P/cm^3, $T = 1.25°$K, $H \approx 3000\phi$). The center of the $m_I = +\frac{1}{2}$ line was saturated prior to the traversal. In the ENDOR technique the field is set to H_0. An additional rf field flips the spin packets as indicated by the arrows thereby desaturating the electron spin resonance line.
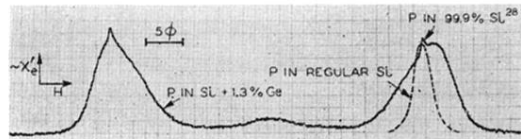
FIG. 20. Electron spin resonance signal from phosphorus-doped silicon with 1.3 atomic percent of germanium. ($T=1.25°$K, $\nu_e \simeq 9000$ Mc/sec). The broadening of the line is due to variations in the value of $|\Psi(0)|^2$. The two markers on the trace were obtained from a separate phosphorus-doped silicon sample with isotopically purified Si^{28}.

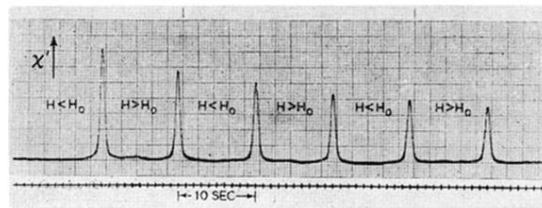FIG. 26. Reduction of the magnetization during successive adiabatic fast passages. The time between two passages is short in comparison to the electron spin relaxation time T_s ($T_s \simeq 40$ minutes). No magnetic field modulation was used to observe the signal. The sample is phosphorus-doped silicon ($\sim 10^{16}$ P/cm³, $T = 1.25°$K, $\nu_e \simeq 9000$ Mc/sec).
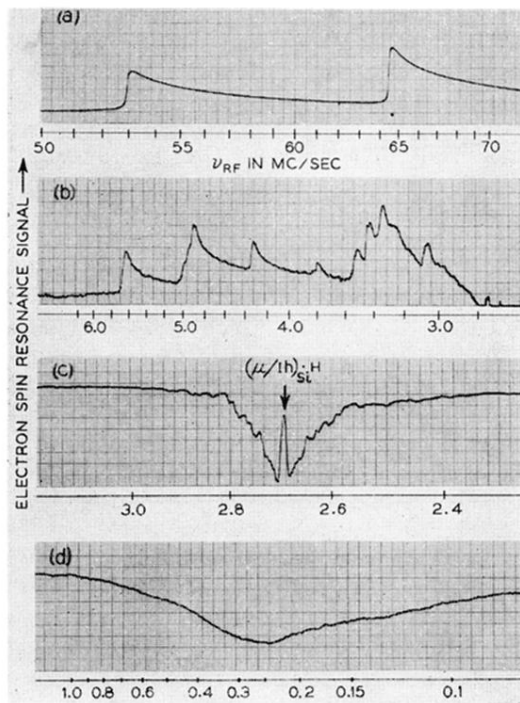
FIG. 3. Variation of the microwave electron spin resonance signal with the application of an additional rf field. The sample is phosphorus-doped silicon (5×10^{16} P/cm³, $T = 1.25°$K, $H_0 \approx 3000$ oersteds). Figure 3(a) shows the increase in signal when the donor hf interaction frequencies are traversed. Figure 3(b) arises from the hf interaction with Si²⁹'s located at different lattice points (see also Figs. 4 and 13). Figure 3(c) is due to the hf interactions with Si²⁹'s which are far removed from the donor. The decrease in signal in Fig. 3(d) is due an effect akin to rotary saturation.[19]
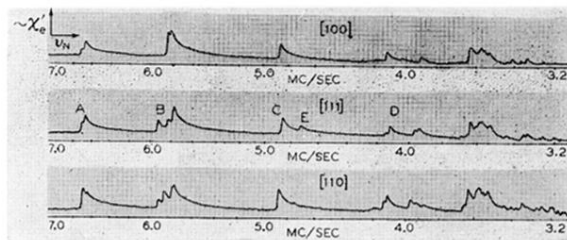
FIG. 4. The ENDOR signal from arsenic-doped silicon (8×10^{16} As/cm^3, $T = 1.25°$K, $\nu_e \approx 9000$ Mc/sec). The lines represent the hf interaction of the donor electron with the Si^{29} nuclei at different lattice points. Note the change in the structure of the lines when the magnetic field points along the different crystalline directions. For the analysis of this anisotropic interaction the rate of frequency sweep was reduced (see Fig. 13).